Supporting Information for

Light Enhanced Fe-Mediated Nitrogen Fixation: Mechanistic Insights Regarding H_2 Elimination, HER, and NH_3 Generation

Dirk J. Schild and Jonas C. Peters*

Division of Chemistry and Chemical Engineering, California Institute of Technology (Caltech), Pasadena, California 91125, United States

Corresponding Author

* jpeters@caltech.edu.

Table of Contents:

Experimental Section

General considerations. All manipulations were carried out using standard Schlenk or glovebox techniques under an N_2 atmosphere. Unless otherwise noted, solvents were deoxygenated and dried by thoroughly sparging with argon gas followed by passage through an activated alumina column in the solvent purification system by SG Water, USA LLC. 2-MeTHF was degassed by three freeze-pump-thaw cycles, followed by drying over NaK to remove traces of water. Deuterated solvents were purchased from Cambridge Isotope Laboratories, Inc., degassed, filtered through an alumina plug, and dried over 3Å molecular sieves prior to use. All reagents were purchased from commercial vendors and used without further purification unless stated otherwise. $P_2P^{Ph}FeBr_2$ (**3**) and $P_2P^{Ph57}FeCl_2$,[1] $[H(OEt_2)_2][BAr^F{}_4]$ ($BAr^F{}_4$ = tetrakis(3,5-bis(trifluoromethyl)phenyl)borate),[2] $Cp^*{}_2Co$,[3] and KC_8[4] were synthesized following literature procedures.

Physical Methods.

NMR spectra were recorded at room temperature unless otherwise noted. ^1H, ^{13}C and ^{29}Si chemical shifts are reported in ppm relative to tetramethylsilane, using residual solvent proton and ^{13}C resonances as internal standards. ^{29}Si NMR chemical shifts were determined from 29Si-HMBC two-dimensional spectra ^{15}N and ^{31}P and chemical shifts are reported relative to CH_3NO_2 and 85 % aqueous H_3PO_4 respectively. Solution phase magnetic measurement were performed by the method of Evans.[5]

IR spectra were obtained using a Bruker Alpha Platinum ATR spectrometer with OPUS software in a glovebox under an N_2 atmosphere.

UV-Vis measurements were collected using a Cary 50 instrument with Cary WinUV software.

X-band EPR spectra were obtained on a Bruker EMX spectrometer on 2-5 mM solutions prepared as frozen glasses in 2-MeTHF. Samples were collected at powers ranging from 20 μW to 2 mW and modulation amplitudes of 1 – 5 Gauss. Spectra were simulated using the Easyspin suite of programs with Matlab 2018.

Mössbauer spectra were recorded on a spectrometer from SEE Co. operating in the constant acceleration mode in a transmission geometry. Spectra were recorded with the temperature of the sample maintained at 80 K. The sample was kept in an SVT-400 Dewar from Janis. The quoted isomer shifts are relative to the centroid of the spectrum of a metallic foil of α-Fe at room temperature. Data analysis was performed using the program WMOSS (www.wmoss.org) and quadrupole doublets were fit to Lorentzian lineshapes.

Cyclic voltammetry measurements were carried out in a glovebox under an N_2 atmosphere in a one-compartment cell using a CH Instruments 600B electrochemical analyzer. A glassy carbon electrode was used as the working electrode and a carbon rod was used as the auxiliary electrode. The reference electrode was AgOTf/Ag in THF isolated by a CoralPor™ frit (obtained from BASi). The ferrocenium/ferrocene couple (Fc^+/Fc) was used as an external reference. THF solutions of electrolyte (0.1 M $[NBu_4][PF_6]$) and analyte were also prepared under an inert atmosphere.

Hydrogen Analysis. The headspace of reaction flasks was analyzed by gas chromatography to quantify H_2 evolution with an Agilent 7890A gas chromatograph (HPPLOT U, 30 m, 0.32 mm i.d., 30 °C isothermal, 1 mL/min flow rate, N_2 carrier gas) using a thermal conductivity detector.

X-Ray Crystallography. X-ray diffraction studies were carried out at the Caltech Division of Chemistry and Chemical Engineering X-ray Crystallography Facility on a Bruker three-circle SMART diffractometer with a SMART 1K CCD detector, APEX CCD detector, or Bruker D8 VENTURE Kappa Duo PHOTON 100 CMOS detector. Data were collected at 100 K using Mo Kα radiation (λ = 0.71073 Å) or Cu Kα radiation (λ = 1.54178 Å). Structures were solved by direct or Patterson methods using SHELXS and refined against F2 on all data by full-matrix least squares with SHELXL-97.68 All non-hydrogen atoms were refined anisotropically. All hydrogen atoms were placed at geometrically calculated positions and refined using a riding model. The isotropic displacement parameters of all hydrogen atoms were fixed at 1.2 (1.5 for methyl groups) times the Ueq of the atoms to which they are bonded. See below for any special refinement details for individual data sets.

Combustion analysis measurements were collected using a PerkinElmer 2400 Series II CHN Elemental Analyzer.

Computational methods Geometry optimizations were performed using the Gaussian09 package all optimizations.[6] The TPSS functional[7] was employed in combination with def2-TZVP[8] basis set on transition metals and a def2-SVP[8] basis set for all remaining atoms in frequency calculations and geometry optimizations.

Experimental

P_2P^{Ph}: A 1.6 M *n*-BuLi solution (6.5 mL, 10.4 mmol) was added dropwise to a stirring solution of (2-bromophenyl)diisopropylphosphine (2.83 g, 10.3 mmol) in 40 mL diethyl ether at -78 °C. Following the addition,the light-yellow reaction mixture was stirred for 90 minutes at -78 °C. *P,P*-dichlorophenylphosphine (0.924 g, 5.1 mmol) in 6 mL diethyl ether was added over 30 minutes, resulting in a color change to red. The yellow suspension obtained after warming to room temperature overnight, was brought into the glovebox and filtered over celite. The flask was rinsed four times with 8 mL diethyl ether and the resulting solutionswere subsequently passed over celite and combined with the filtrate. The solvent of the combined filtrates was removed *in vacuo*, yielding a pale yellow powder. The powder was washed with pentane (3 x 5 mL) and dried under vacuum to give P_2P^{Ph} (**1**) as a white solid (1.23 g, 2.5 mmol, 47 %) evident by comparing spectroscopic properties with previously reported spectra.[1] ^{1}H NMR (Benzene-d_6, 400 MHz) δ ppm 7.49 – 7.40 (m, 2H), 7.39 – 7.31 (m, 2H), 7.08 (t, J = 6.7 Hz, 7H), 6.97 (t, J = 7.5 Hz, 2H), 2.11 (td, J = 7.0, 2.6 Hz, 2H), 1.98 (hept, J = 7.1 Hz, 2H), 1.18 (td, J = 13.8, 7.0 Hz, 12H), 0.92 (ddd, J = 32.8, 11.5, 7.0 Hz, 12H). ^{13}C NMR (C_6D_6, 101 MHz) δ ppm 148.42 (m), 142.42 (m), 139.73 (dt), 135.64 (d), 134.88 (m), 132.44 (m), 128.91 (s), 128.45 (d), 24.94 (m), 20.56 (m), 19.88 (m). ^{31}P{1H} (C_6D_6, 162 MHz) δ ppm -2.17 (dd, $^3J_{PP}$ = 158.7, $^3J_{PP}$ = 147.0 Hz, 2P, P-Ar), -14.26 (dt, $^3J_{PP}$ = 158.7, $^3J_{PP}$ = 147.0 Hz, 1P, P-Ph).

(P_2P^{Ph})FeBr (**4**): A dark purple solution of **3** (173.0 mg, 243 μmol) dissolved in 8 mL THF was stirred over sodium amalgam (5.8 mg, 252 μmol) for 2 h at room temperature during which the color changed to dark red. The red solution was filtered over celite and dried *in vacuo*. The resulting red solid was extracted with 4 mL Et_2O and filtered over celite. Washing the red solid 4 times with 1.5 mL pentane yielded P_2P^{Ph}FeBr as a red solid (99.8 mg, 158 μmol 65%). Crystals suitable for XRD were obtained by vapor diffusion of pentane into a benzene solution of P_2P^{Ph}FeBr. ^{1}H NMR (400 MHz, Benzene-d_6) δ 124.74 (2H), 104.79 (2H), 17.85 (2H), 7.96 (6H), 6.46,4.89, 3.84 (2H), 2.41 (2H), 1.02 (2H), -2.64 (6H), -7.19 (6H), -17.74 (2H), -20.57 (1H). UV-Vis (Benzene, nm {cm^-

[1] M^{-1}}): 320 {6950}, 375 {5225}, 433 {4785}, 830 {1315}. μ_{eff} (C_6D_6, Evans Method, 25 °C): 4.11 μ_B. Anal: calculated for $C_{30}H_{41}BrFeP_3$: C 57.17, H 6.56 found: C 56.83, H 6.58

[(P_2P^{Ph})Fe(H)]$_2$(μ–N_2) (1): A 20 mL vial containing **4** (97.4 mg, 154.5 μmol) in 10 mL toluene was cooled down to −78 °C. 6.1 mL of an 0.25 M $NaHBEt_3$ solution in toluene was added after which the mixture was stirred at -78 °C for 30 minutes followed by 2 h at room temperature. Upon warming to room temperaturethe color changed from dark red to forest green. The solvent was removed *in vacuo*, after which the residue was extracted with 6 mL pentane. Reducing the solvent to 3 mL and storing at −35 °C yielded **1** as green crystals (50.1 μmol, 61 %), as was evident by comparing the spectroscopic properties with previously reported spectra.[1] 1H NMR (THF-d_8, 500 MHz) δ ppm 8.15 (d, J = 7.5 Hz, 2H), 7.52 (d, J = 7.5 Hz, 2H), 7.43 (t, J = 7.3 Hz, 2H), 7.26 (t, J = 7.3 Hz, 2H), 7.14 (t, J = 7.3 Hz, 2H), 6.63 (d, J = 7.4 Hz, 2H), 6.12 (t, J = 7.5 Hz, 1H), 2.99 (broad s, 2H), 2.59 (broad s, 2H), 0.72 (m, 6H), 0.42 (m, 6H).

(P_2P^{Ph})Fe(N_2)$_2$ (5) from 3: 50 mL of a THF solution of **3** (555.8 mg, 782 μmol) was stirred over sodium mercury amalgam (36.7 mg, 1.596 μmol, 9.6 g Hg) for 16 h at room temperature during which the color changed to wine red. The THF solution was filtered over celite, and the solvent was subsequently removed *in vacuo*. The material was extracted with pentane 40 mL and filtered over celite. Cooling down the filtrate down to −35 °C yields crystalline $P_2P^{Ph}Fe(N_2)_2$ (205.2 mg, 339 μmol 43%). Additional product can be obtained by cooling down the concentrated mother liquor. No satisfactory elemental analysis could be obtained, with C and H percentages slightly higher than expected. The nitrogen content was consistently low, which is likely due to the loss of an N_2 ligand. The equilibrium discussed in the main text also hampers obtaining quantitative integrals in certain regions. ^{1}H NMR (400 MHz, Benzene-d_6) δ 7.63 (t, J = 6.3 Hz, 2H), 7.50 (dd, J = 6.0, 3.9 Hz, 2H), 7.12 – 6.75 (m, 9H), 2.86 – 2.53 (m, 4H), 1.57 – 1.40 (m, 6H), 1.35 – 0.96 (m, 18H), ^{13}C NMR (101 MHz, THF) δ 147.69, 131.47, 130.21, 129.07, 128.66, 127.29, 32.49, 27.99, 19.29, 18.84, ^{31}P NMR (162 MHz, Benzene-d_6) δ 122.76 (t, J = 63.0 Hz, 1H), 100.26 (d, J = 63.0 Hz 2P). IR (ATR, THF C_6D_6 film): νN_2 = 2065 cm^{-1}, 2005 cm^{-1}. UV-Vis (Et_2O, nm {cm^{-1} M^{-1}}): 251 {25000}, 322 {8816}, 405 {5480}, 490 {3820}, 830

(P_2P^{Ph})Fe(N_2)$_2$ (5) from 4: A 7 mL THF solution of **4** (81.0 mg, 128 μmol) was stirred over sodium mercury amalgam (3.6 mg, 156 μmol) for 1 hour and subsequently filtered over celite. THF was remove *in vacuo* and the residue was extracted with 6 mL pentane and filtered over celite. Cooling the solution to −35 °C yields $P_2P^{Ph}Fe(N_2)_2$ as a crystalline solid (37.8 mg, 62 μmol, 48%). Additional product can be obtained by cooling down the concentrated mother liquor.

(P_2P^{Ph})^{57}Fe(N_2)$_2$ (^{57}5): Complex ^{57}**5** was prepared using the synthetic procedure for **5** with $P_2P^{Ph57}FeCl_2$ instead. The ^{1}H NMR spectrum matched that of **5**, while additional coupling with ^{57}Fe was present in the ^{31}P NMR spectrum. ^{31}P NMR (162 MHz, Benzene-d_6) δ 122.76 (dt, $^2J_{PP}$ = 64.5 Hz, $^1J_{FeP}$ = 46.2 Hz, 1P), 100.26 (t, J = 63.0 Hz, 2P).

[(P_2P^{Ph})Fe]$_2$μ–N_2 (6): An NMR tube containing **5** (20.5 mg, 33.8 μmol) in 0.6 mL toluene-d_8 was freeze-pump thawed three times, stored for 4 hours and freeze-pump thawed three additional times. A ^{31}P NMR spectrum was recorded to ensure full conversion to **6**. During the cycles, the color changes from maroon to a dark purple. If **5** was still present, additional freeze-pump thaw cycles were performed until the signal corresponding to **5** was negligible. Attempts to isolate the product as a crystalline solid were unsuccessful. ^{1}H NMR (500 MHz, Toluene-d_8) δ 7.97 (d, J = 7.4 Hz, 2H), 7.44 (d, J = 7.3 Hz, 2H), 7.31 (dd, J = 7.3 Hz, J = 7.3 Hz, 2H), 6.94 (dd, J = 7.4 Hz, J = 7.3 Hz, 2H), 6.87 (dd, J = 7.3 Hz, J = 7.3 Hz, 2H), 6.46 (s, 2H), 5.79 (s, 1H), 5.35 (s, 2H), 5.07 (s,

2H), 1.61 (s, 6H), 1.05 (s, 6H), 1.01 (s, 6H) 0.43 (s, 6H).^{31}P NMR (202 MHz, Toluene-d_8, 298 K) δ 184.84. ^{31}P NMR (202 MHz, Toluene-d_8, 203 K) δ 130.42, 123.63 Small amounts of an unknown species are present at 98.05 and 92.51 ppm, but they account for less than 5%

(P_2P^{Ph})Fe(N_2)($H)_2$ (2): A Schlenk tube containing **5** (60.9 mg, 100 µmol) in THF (6 mL) was freeze-pump-thawed 3 times and exposed to 1 atmosphere of H_2. The reaction was stirred vigorously at room temperature for 24 hours before it was freeze-pump-thawed 2 times, re-exposed to 1 atmosphere of N_2, and stirred for another 24 hours, during which thesolution turned yellow. The solvent was removed *in vacuo*, yielding **2** quantitatively (58.0 mg, 100 µmol, 100%). The nature of the solid was determined by comparing its NMR and IR features with those reported.[1] ^{1}H NMR (THF-d_8, 500 MHz) δ ppm 8.09 (t, J = 6.4 Hz, 2H), 7.77 (d, J = 7.2 Hz, 2H), 7.40 (p, J = 7.2 Hz, 4H), 7.22–7.15 (m, 5H), 2.67 (h, J = 6.8 Hz, 2H), 2.56–2.50 (m, 2H), 1.43 (q, J = 7.0 Hz, 6H), 1.15–1.19 (m, 12H), 0.46 (q, J = 6.9, 6H), -9.43 (td, J = 38.2 , 15.7 Hz, 1H), -20.71 (td, J = 43.2 , 15.6 Hz, 1H), ^{31}P NMR (162 MHz, Benzene-d_6) δ ppm 119.2 (2P), 110.2 (1P). IR (ATR, THF C_6D_6 film): 2071 cm^{-1} (νN_2), 1796 cm^{-1} (νFe–H).

[(P_2P^{Ph})Fe(N_2)$_2$(H)][BAr^F_4] (7): A 20 mL vial containing **1** (16.4 mg, 14.5 µmol) in 1.5 mL diethyl ether was cooled down to −78 °C. A cooled solution of $FcBAr^F_4$ (32.8 mg, 31.2 µmol) in 1.5 mL diethyl ether was added dropwise during which the color changes from green to orange. The solution was stirred at −78 °C for 1 hour and warmed to room temperature. The mixture was subsequently filtered over celite. The filtrate was layered with 10 mL pentane and stored at −35 °C overnight, which resulted in the formation of orange crystals (41.0 mg, 27.8 µmol 96 %). The obtained crystalline material was suitable for X-ray diffraction. ^{1}H NMR (THF-d_8, 400 MHz) δ ppm 8.22–8.10 (m), 7.85–7.69 (m), 7.59–7.50 (m), 7.36 (t, J = 7.9, 1H), 7.30–7.27 (m), 7.27–7.21 (m), 6.60 (t, J = 9.3 Hz, 2H), 3.14–2.92 (m, 4H), 1.56–1.41 (m), 1.35–1.14 (m), -16.85 (dt (q), J = 54.9, 1H). ^{11}B NMR (THF-d_8, 128 MHz) δ ppm -4.68 (s). ^{19}F NMR (THF-d_8, 376 MHz) δ ppm -61.51 (s). ^{31}P{^{1}H} (THF-d_8, 162 MHz) δ ppm 113.41 (overlapping dt, J = 34.6, 25.0 Hz, 103 1P, PPh), 95.75 (dd, J = 29.5, 7.5 Hz, 2P, P*i*Pr$_2$). IR (thin film from evaporation of THF-d_8; cm^{-1}): 2193 (νN–N), 2162 (νN–N), 2069 (νFe–H). UV-Vis (Et_2O, nm {cm^{-1} M^{-1}}): 367{2200} Anal: calculated for $C_{62}H_{54}BF_{24}FeN_4P_3$: C 50.64, H 3.70 N 3.81, found: C 50.23, H 4.00, N 3.17

[(P_2P^{Ph})Fe(N_2)(H)][K(18-crown-6] (8): A 4 mL vial containing **1** (28.4 mg, 25 µmol) in THF was cooled down to −78 °C. Simultaneously, a 20 mL vial containing KC_8 (7.0 mg (51 µmol) and a stir bar was cooled down. After 20 minutes, the THF solution containing **1** was rapidly added to the vial containing KC_8. The mixture is stirred for 45 minutes at −78, after which 18-crown-6 (20.4 mg, 77 µmol) was added. The solution was stirred an additional 45 minutes at room temperature, layered with 6 mL pentane and stored at −35 °C. Over four days black crystals formed suitable for XRD, (35.4 mg, 40 µmol, 90%). ^{1}H NMR (400 MHz, THF-d_8) δ 7.75 (q, *J* = 4.2 Hz, 2H), 7.43 (t, *J* = 4.2 Hz, 2H), 7.24 (t, *J* = 7.6 Hz, 2H), 7.04 – 6.88 (m, 6H), 6.83 (t, *J* = 7.2 Hz, 1H), 2.53 (d, *J* = 9.2 Hz, 2H), 2.42 – 2.26 (m, 2H), 1.24 (ddt, *J* = 21.2, 13.8, 6.6 Hz, 6H), 0.88 (q, *J* = 6.8 Hz, 12H), 0.29 (q, *J* = 6.6 Hz, 6H), -9.69 (td, *J* = 68.8, 67.9, 27.3 Hz, 1H).^{31}P NMR (162 MHz, THF-d_8) δ ppm 120.62 (m, 1P) 119.89 – 118.98 (m. 2P). IR (thin film from evaporation of THF-d_8; cm^{-1}): 1924 (νN–N), 1733 (νFe–H) Anal: calculated for $C_{62}H_{54}BF_{24}FeN_4P_3$: C 57.86, H 7.81 N 2.93, found: C 57.23, H 7.34, N 1.89

[(P_2P^{Ph})Fe(N_2)][K(18-crown-6] (9): A 20 mL vial containing **5** (20.6 mg, 34 µmol) in 1.5 Ml THF was cooled down to −78 °C and 340 µL of a 100 µM potassium naphthalide solution (34 µmol) was added after which the species was stirred. After one hour of stirring, an excess 18-crown-6 was added (18 mg, 68 µmol). The solution was stirred for an hour at room temperature and subsequently layered with 6 mL pentane. Storing the solution in the freezer for 24 h resulted in the formation of dark crystals suitable for XRD (20.9 mg, 23.8 µmol 70%). ^{1}H NMR (400 MHz, THF-d_8) δ 63.91 26.76, 20.51, 18.28, 13.61. 9.85, 6.27, 5.22, 1.04, -2.15, -7.78, -27.16 ppm. IR (ATR, THF C_6D_6 film): 1872 cm^{-1} (νN_2), Anal: calculated for $C_{62}H_{53}BF_{24}FeN_4P_3$: C 57.64, H 7.61 N 2.93, found: C 57.23, H 7.34, N 1.89

[(P_2P^{Ph})Fe(N_2)][K_2(THF)$_3$] (10): A 20 mL vial containing **5** (120.1 mg, 198 µmol) dissolved in 5 mL NaK dried THF was cooled down to −78 °C. Simultaneously, a 20 mL vial containing KC_8 (80.2 mg, 600 µmol) and a stir bar was cooled down to −78 °C. The cooled solution containing **5** was added to the vial containing KC_8 after which the vial was rinsed with 0.5 mL THF which was subsequently added. The solution was stirred for 15 minutes. and filtered over celite. To assure the frit and celite are sufficiently dry, 3 mL NaK dried THF was passed through the frit four times before the reaction mixture was passed over celite. The reaction vial was rinsed with 1 mL THF, and the wash was passed over celite. The filtrate was divided into two 20 mL vials and each vial was layered with 15 mL pentane. Crystals of **10** suitable for XRD formed over a period of a week. (110.1 mg, 126 µmol, 63%). ^{1}H NMR (400 MHz, THF-d_8) δ 7.87 (m, 2H), 7.51 – 7.34 (m, 2H), 6.89 (m, 8H), 6.71 (t, J = 7.2 Hz, 1H), 2.90 – 2.58 (m, 2H), 2.58 – 2.38 (m, 2H), 1.29 (m, J = 12H), 0.81 (q, J = 5.8 Hz, 6H), 0.23 (q, J = 5.9 Hz, 6H). ^{13}C NMR (101 MHz, THF-d_8) δ 157.27, 154.67, 153.04, 131.46, 129.79, 128.62, 128.05 – 122.99 (m), 35.82, 29.23, 24.12 – 19.34 (m). ^{15}N NMR (41 MHz, THF-d_8) δ 2.36, -25.91. ^{31}P NMR (162 MHz, THF-d_8) δ 113.13 (d, J = 33.8 Hz), 95.15 (t, J = 33.8 Hz). No satisfactory combustion analysis could be obtained.

[(P_2P^{Ph})Fe(NNSiMe$_3$)]K (11- NNSiMe$_3$)K: A 20 mL vial containing **5** (55.9 mg, 92 µmol, in 5 mL NaK dried THF was cooled down to -78 °C in a glovebox Coldwell after which it was added to a vial containing KC_8 (37.4mg, 276 µmol 3 equiv.) at -78 °C, Stirring the solution for 30 minutes resulted in a color change to dark purple. The cold suspension was filtered over celite, and subsequently cooled down to -78 °C followed by the addition of TMSCl (11.6 µL, 92 µmol) which resulted in an immediate color change to brown. The mixture was subsequently stirred at −78 °C for 30 minutes, followed by 30 minutes at room temperature. Volatiles were removed *in vacuo* and the residue was dissolved in benzene and filtered over celite. Benzene was removed *in vacuo*, and the solid washed with pentane (3 x 2 mL) and filtered over a celite plug. The remaining solids were dissolved in diethyl ether and passed over the same celite plug. Removal of diethyl ether *in vacuo* yields [P_2P^{Ph}Fe(NNTMS)]K (35 mg, 54 µmol, 58%). Crystals suitable for XRD could be grown by layering a concentrated benzene solution with pentane. ^{1}H NMR (C_6D_6, 400 MHz): δ 7.84 (m, 2H), 7.68 (d, $^3J_{HH}$ = 6.69 Hz, 2H), 7.10-6.96 (m, 6H), 6.66-6.42 (m, 3H), 2.99-2.76 (m, 2H), 2.31-2.17 (m, 2H), 1.59-1.40 (m, 6H), 1.33-0.89 (m, 18H), 0.38 (s, 9H, Si(CH_3)$_3$); ^{29}Si NMR (79 MHz, C_6D_6, HMBC) δ: 4.72 (s, N-SiCH3). ^{13}C NMR (101 MHz, C_6D_6) δ 130.65 (d, *J* = 10.4 Hz), 127.98, 127.54 (d, *J* = 6.0 Hz), 126.48 – 125.86 (m), 125.54 (d, *J* = 11.5 Hz), 32.72 (t, *J* = 9.4 Hz), 28.26 (d, *J* = 8.4 Hz), 21.36 – 19.79 (m), 0.98, -1.11. ^{31}P NMR (162 MHz, C_6D_6) δ 117.48 (d, *J* = 16.7 Hz, 2P, PAr), 109.12 (t, *J* = 16.6 Hz, 1P, PPh). Anal: calculated for $C_{33}H_{56}FeKN_2P_3Si$: C 57.38, H 7.81 N 4.06, found: C 57.17, H 7.07, N 3.61

[(P_2P^{Ph})Fe(NNSi^{i}Pr$_3$)]K (11-NNSi^{i}Pr$_3$): $P_2P^{Ph}Fe(N_2)_2$ (50.1 mg, 83 µmol) in 2.5 mL NaK dried THF was cooled down to −78 °C in a glovebox coldwell and passed over a pipette with a thin layer of KC_8 (4 mm). The mixture was passed over the pipette three times during which the color changed to dark purple. TiPSOTf (20 µL, 74 µmol was added upon which an immediate color change to orange brown was observed. The mixture was subsequently stirred at −78 °C for 30 minutes, after which it was taken out of the coldwell and stirred at room temperature for 30 minutes. Volatiles were removed *in vacuo* and the residue was dissolved in benzene and filtered over celite. Benzene was removed *in vacuo* and the remaining residue washed with HMDSO (5 x 1.5 mL) and filtered over celite. The remaining brown residue in the vial and on the celite was dissolved in diethyl ether. Removal of diethyl ether *in vacuo* yields $[P_2P^{Ph}Fe(NNT\textit{i}PS)]K$ in 75 % yield (43.0 mg, 55 µmol). ^{1}H NMR (300 MHz, Benzene-d_6) δ 7.89 (s, 3H), 7.69 (d, J = 6.7 Hz, 2H), 7.09, (s, 6H), 6.62 (s, 3H), 3.55 (s, 3H) 2.88 (s, 2H), 2.62 (s, 2H), 1.50 (td, J = 14.5, 13.7, 6.4 Hz, 12H), 1.38 – 1.14 (m, 35H), 0.97 – 0.81 (m, 12H). ^{31}P NMR (121 MHz, Benzene-d_6) δ 118.22 (d, J = 17.9 Hz), 111.69 (t, J = 17.9 Hz). IR (ATR, C_6D_6 film): 1469 cm^{-1} (νN_2),

Stochiometric reactivity

Addition of H_2 to 5 at -78 °C. The headspace of a J-Young NMR tube containing **5** (5.9 mg, 9.7µmol) was degassed once by a freeze-pump-thaw cycle. The tube was warmed transferred into a dry ice acetone bath and one atmosphere of H_2 was added. The cold tube was rapidly shaken for 5 seconds and inserted into the precooled NMR spectrometer.

Addition of H_2 to 6 at -78 °C. To a J-Young NRM tube containing **6**, generated *in situ* according to the preparation described above, was added one atmosphere of H_2. The cold tube was rapidly shaken for 5 seconds and inserted into the precooled NMR spectrometer.

General procedure for the synthesis of [(P_2P^{Ph})Fe(N_2)$_2$(H)][BAr^F_4] (7) from 1, 2 or 5 with $HBAr^F_4$: A 20 mL vial containing **1**, **2**, or **5** (9.4 µmol for **1**, 18.8 µmol for **2** and **5**) in diethyl ether (1 mL) was chilled to −78 °C in the glovebox coldwell. In a separate 4 mL vial, a diethyl ether solution of $HBAr^F_4$ (0.019 g, 18.4 µmol, 250 µL diethyl ether) was chilled to −78 °C. Both solutions were allowed to cool for 20 min before the $HBAr^F_4$ solution was added to the vial containing **1**, **2** or **5** at -78 °C in one shot. The vial containing $HBAr^F_4$ was subsequently rinsed with 250 µL of pre-chilled diethyl ether and the rinsing was added to the vial containing. The reaction mixture was stirred at −78 °C for 1 hour and 15 minutes before it was warmed to warm to room temperature. Analysis by NMR and IR spectroscopy confirms the nature of the product as **7**.

NMR analysis of addition of $HBAr^F_4$ to 5 at -78 °C: **5** (5.9 mg, 9.7µmol) was dissolved in 0.4 mL THF-d_8 and added to a J-Young NMR tube at −78 °C. $HBAr^F_4$ (10.3 mg, 10.7 µmol) was cooled to −78 °C and added to the NMR tube. The cold tube was rapidly shaken for 5 seconds, taken out of the glovebox and inserted into the precooled NMR spectrometer at −78 °C.

Oxidation of [(P_2P^{Ph})Fe(NNSiMe$_3$)]K at room temperature. To a stirring solution of $[P_2P^{Ph}Fe(NNTMS)]K$ (13.0 mg, 17 µmol) in 3 mL THF was added [Cp*$_2$Co][PF_6] (8.2 mg, 17 17 µmol) suspended in 1 mL THF. The mixture was stirred for 24 hours, followed by removal of the solvent *in vacuo*. Extracting the solid twice with 5 mL pentane results in an off-white residue. The pentane extracts were combined and removal of the solvents *in vacuo* gives a brow solid (10 mg). Analysis of the solid by NMR spectroscopy reveals the presence of **5** and cobaltocene.

Oxidation of [(P_2P^{Ph})Fe(NNSiMe$_3$)]K (11-NNSiMe$_3$) at −78 °C. To a cooled stirring solution of [(P_2P^{Ph}) Fe(NNTMS)]K (4 µmol) in 1 mL 2-MeTHF at −78 °C was added [Cp*$_2$Co][PF_6] (8.2 mg, 17 µmol) suspended in 0.5 mL 2-MeTHF. The solution was stirred for 5 minutes at −78 °C after which the sample was frozen. The frozen solution was briefly thawed and a 300 µL aliquot was transferred to a precooled EPR tube which was subsequently frozen. Additional EPR spectra were recorded for the frozen samples stored at −78 °C for 24 hours.

(P_2P^{Ph})Fe(NN^{i}Pr$_3$) (12-NN^{i}Pr$_3$): A cooled stirring solution of [(P_2P^{ph}) Fe(NNTiPS)]K (15.0 mg, 19 µmol) in 1 mL was added to [Cp*$_2$Co][PF_6] (9.1 mg, 19 µmol) at −78 °C. The solution was stirred at −78 for 10 minutes followed by 10 minutes at room temperature. The solvent was removed *in vacuo* and the residue extracted with pentane. Filtering over celite and removal of the solvent in vacuo gives a product characterized as **12**–**TiPS**. ^{1}H NMR (300 MHz, Benzene-d_6) δ ^{1}H NMR (400 MHz, THF-d_8) δ 12.22 9.31 7.24 5.90, 4.92, 3.39, 2.36 1.63 – 0.48. IR (ATR, THF film): 1659 cm^{-1} (νN_2),

NMR Spectra

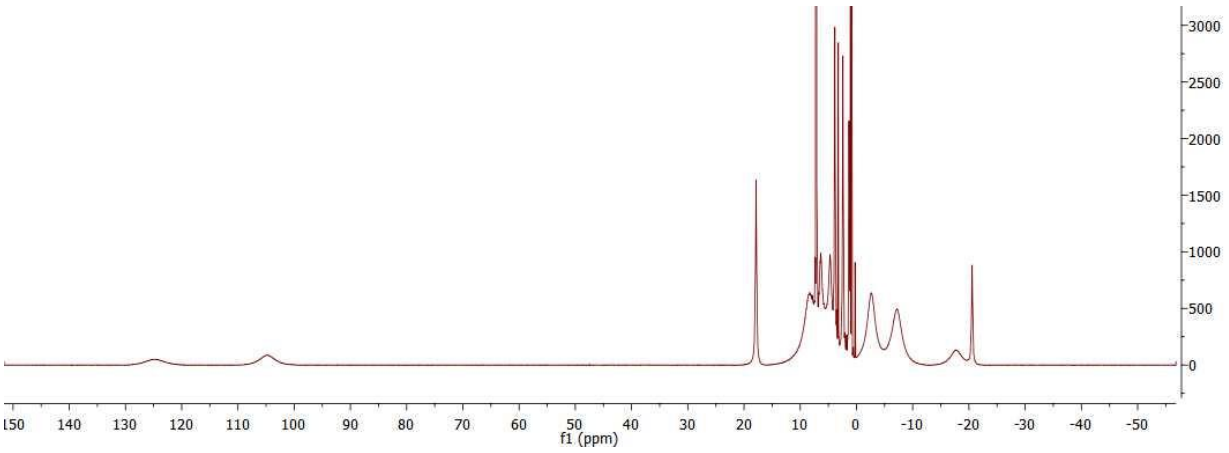

Figure S1 ^{1}H NMR spectrum of (P_2P^{Ph})FeBr (**4**) in C_6D_6 at room temperature

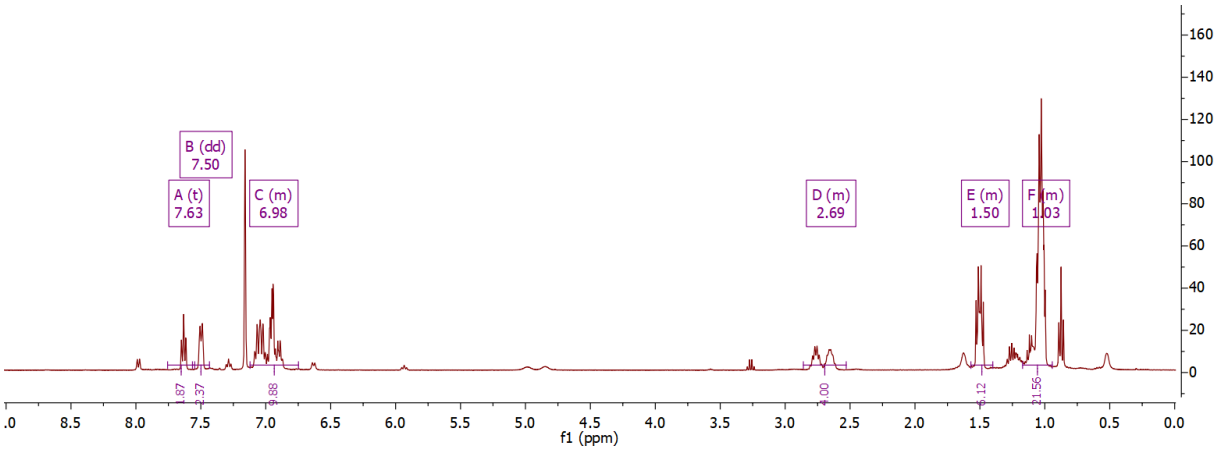

Figure S2 ^{1}H NMR spectrum of (P_2P^{Ph})Fe(N_2)$_2$ (**5**) in C_6D_6 at room temperature. Additional broad peaks corresponding to **6** are present due to the equilibrium as described in the main text.

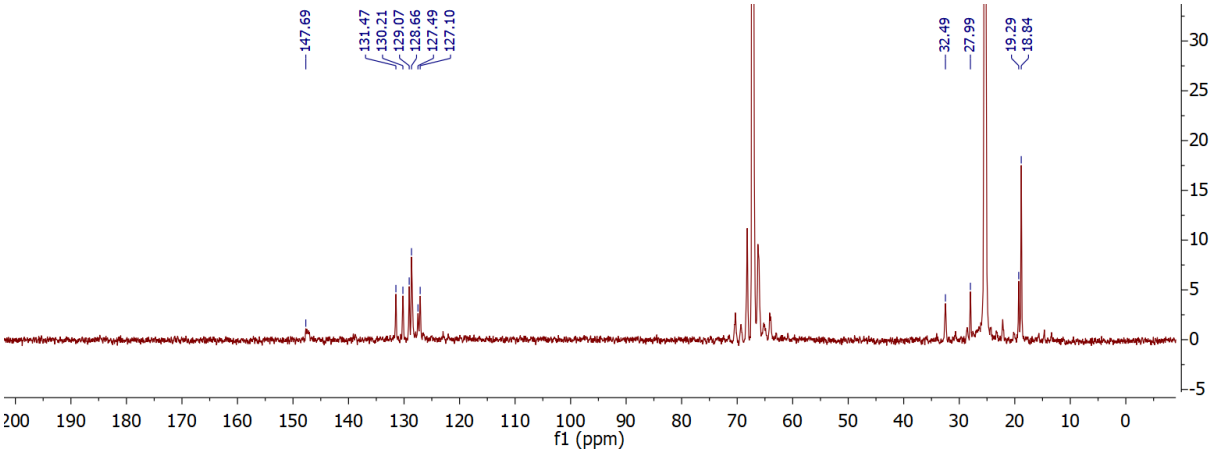

Figure S3 ^{13}C NMR spectrum of (P_2P^{Ph})Fe(N_2)$_2$ (**5**) in THF at room temperature

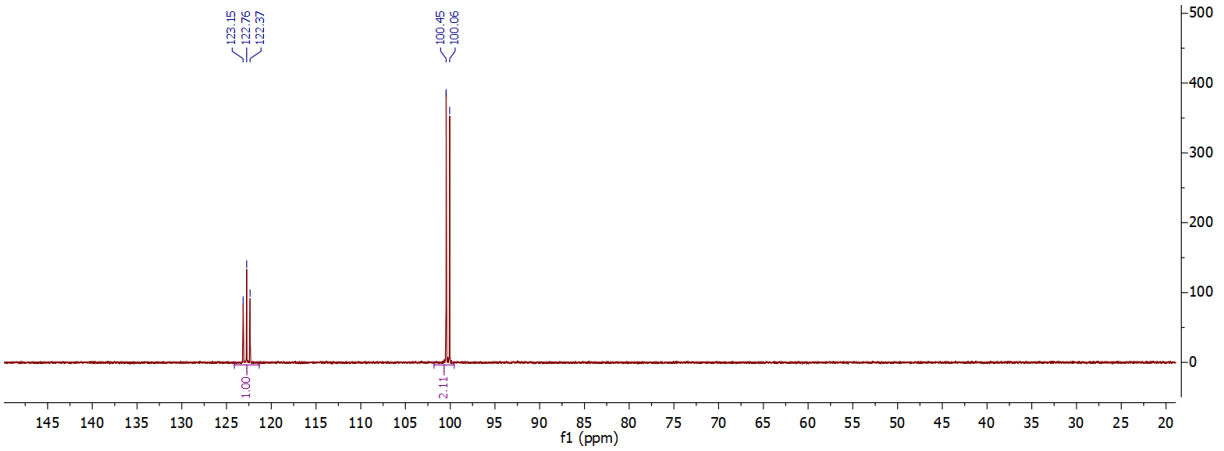

Figure S4 ^{31}P NMR spectrum of $(P_2P^{Ph})Fe(N_2)_2$ (**5**) in C_6D_6 at room temperature

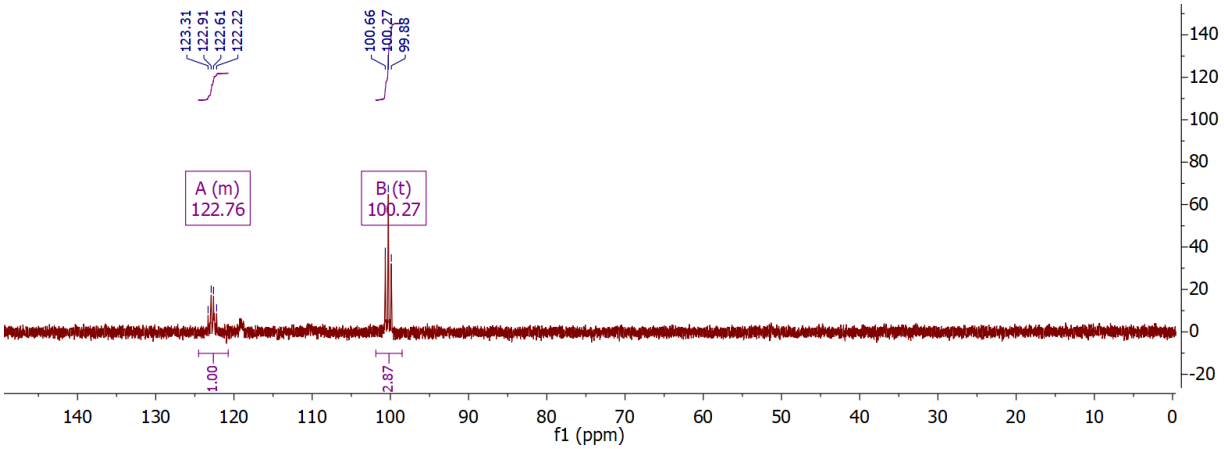

Figure S5 ^{31}P NMR spectrum of $(P_2P^{Ph})^{57}Fe(N_2)_2$ (^{57}**5**) in C_6D_6 at room temperature

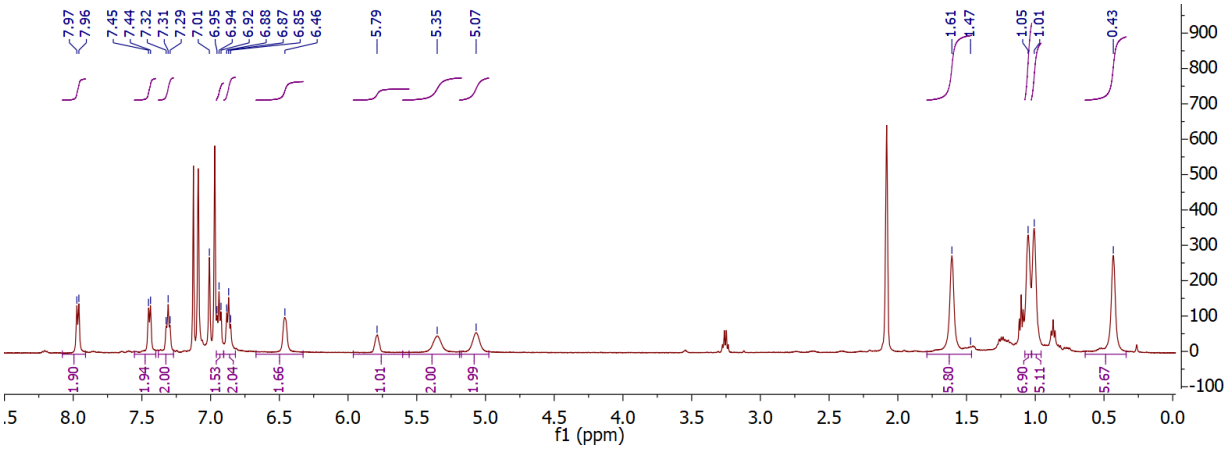

Figure S6 ^{1}H NMR spectrum of $[(P_2P^{Ph})Fe]_2(\mu\text{–}N_2)$ (**6**) in Toluene-d_8 at room temperature

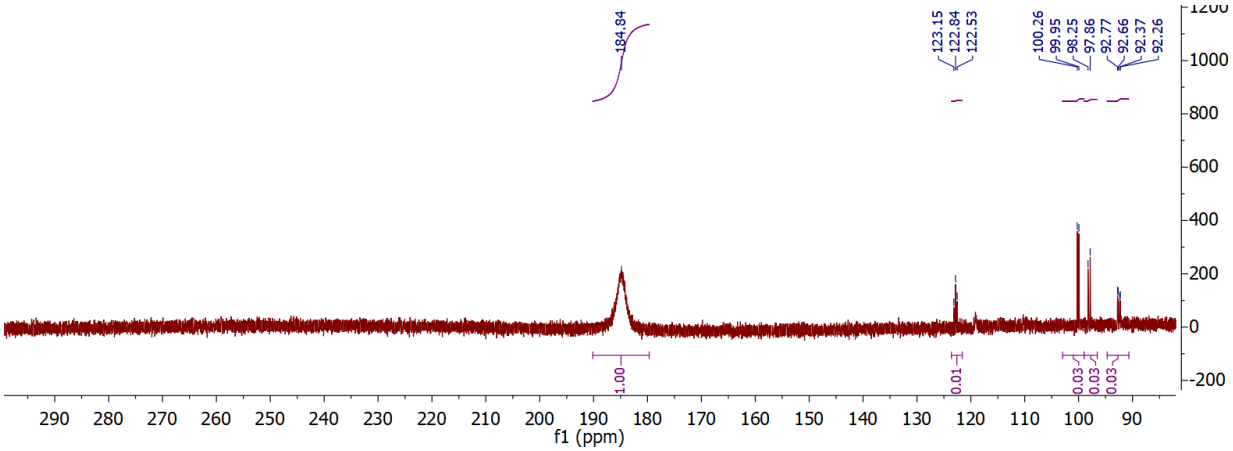

Figure S7 ^{31}P NMR spectrum of $[(P_2P^{Ph})e]_2(\mu\text{–}N_2)$ (**6**) in Toluene-d_8 at room temperature

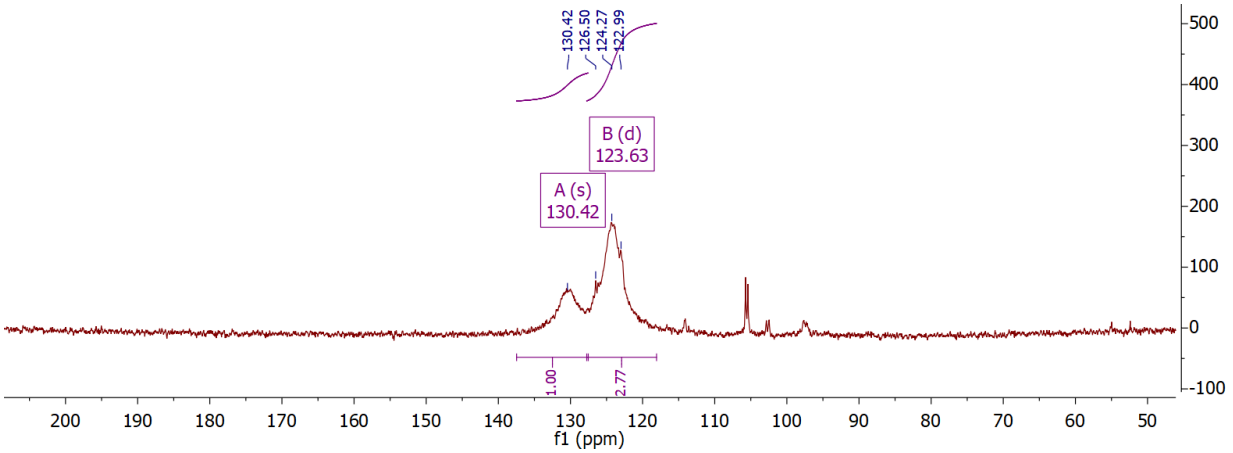

Figure S8 ^{31}P NMR spectrum of $[(P_2P^{Ph})Fe]_2(\mu\text{–}N_2)$ (**6**) in Toluene-d_8 at 203 K

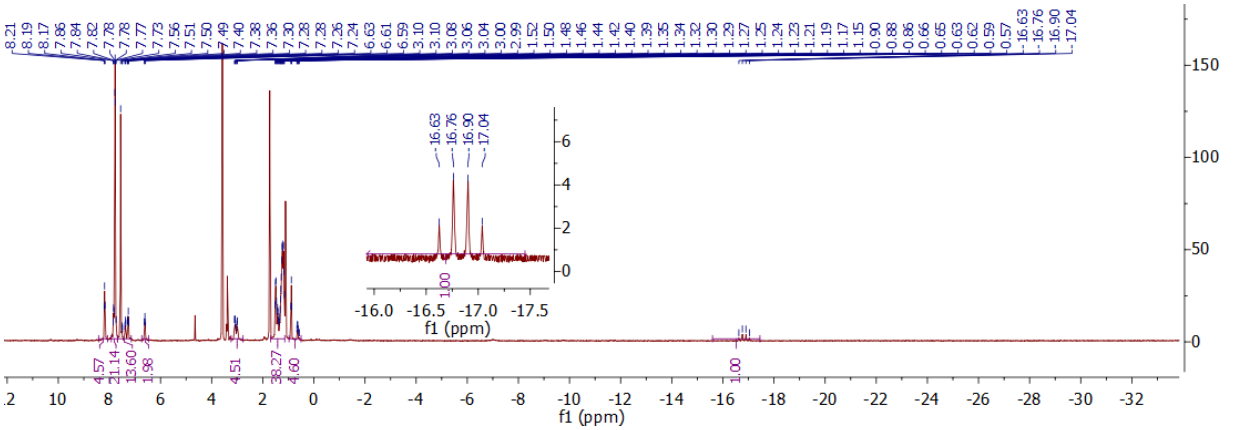

Figure S9 ^{1}H NMR spectrum of $[(P_2P^{Ph})Fe(N_2)_2(H)][BAr^F{}_4]$ (**7**) in THF-d_8 at room temperature

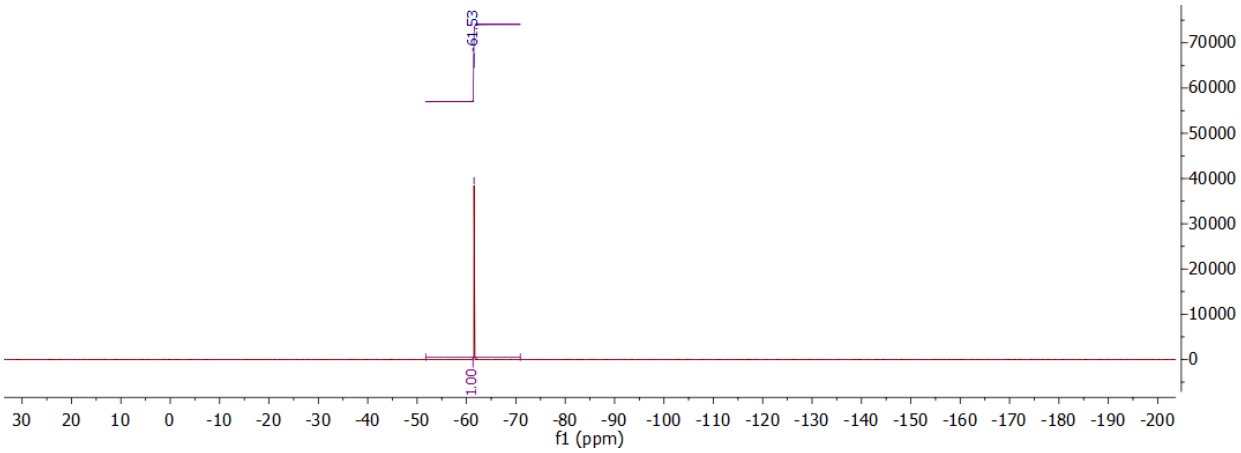

Figure S10 ^{19}F NMR spectrum of [(P_2P^{Ph})Fe(N_2)$_2$(H)][BAr^F_4] (**7**) in THF-d_8 at room temperature

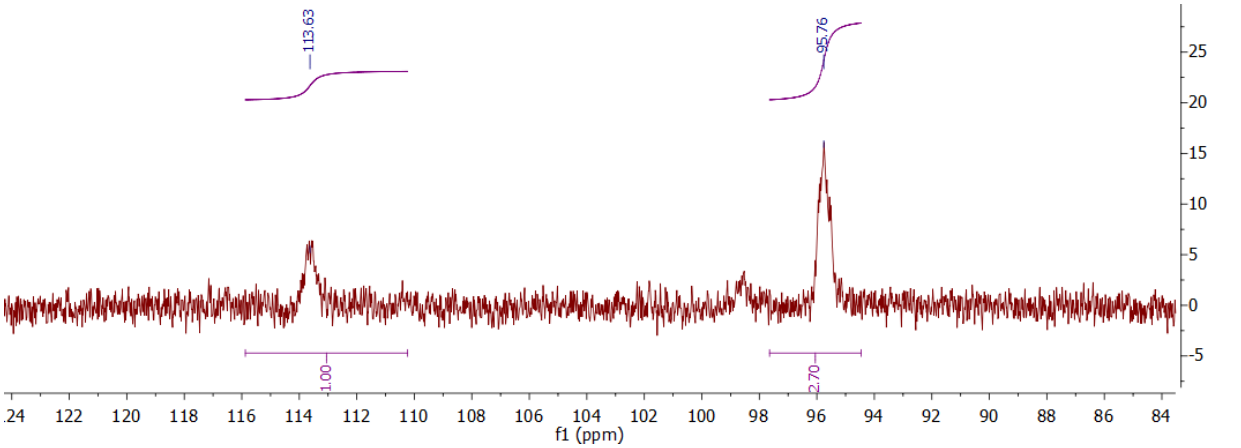

Figure S11 ^{31}P NMR spectrum of [(P_2P^{Ph})Fe(N_2)$_2$(H)][BAr^F_4] (**7**) in THF-d_8 at room temperature

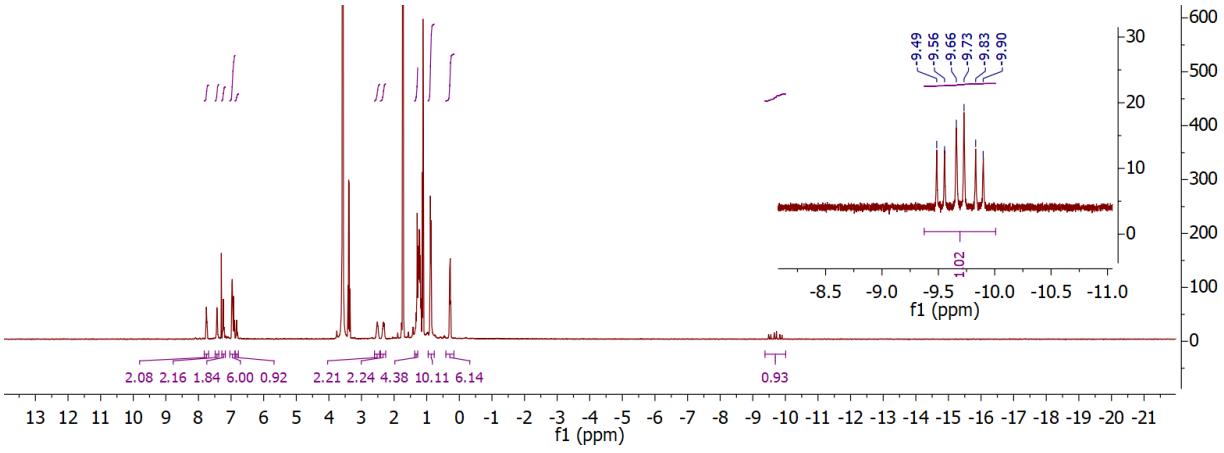

Figure S12 ^{1}H NMR spectrum of [(P_2P^{Ph})Fe(N_2)(H)][K(18-crown-6)] (**8**) in THF-d_8 at room temperature

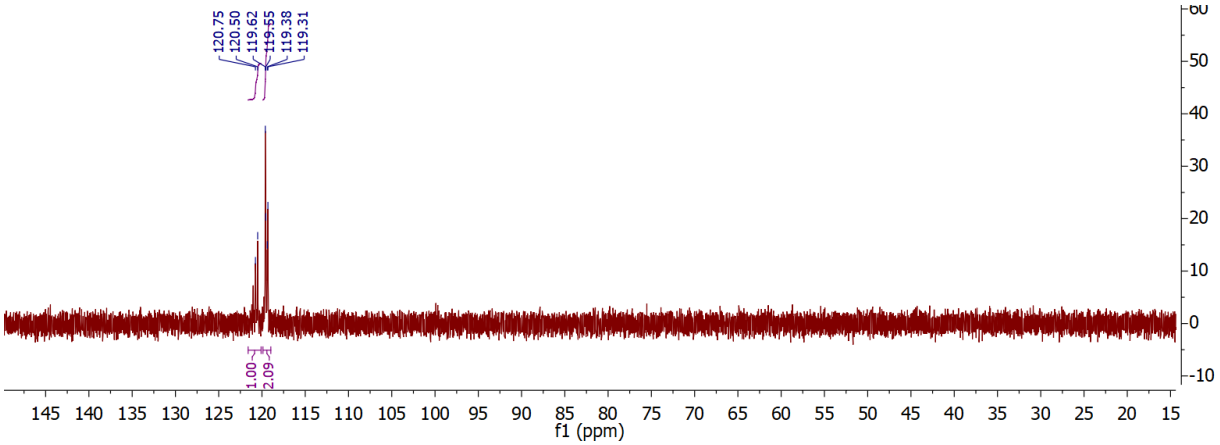

Figure S13 ^{31}P NMR spectrum of [(P_2P^{Ph})Fe(N_2)(H)][K(18-crown-6)] (**8**) in THF-d_8 at room temperature

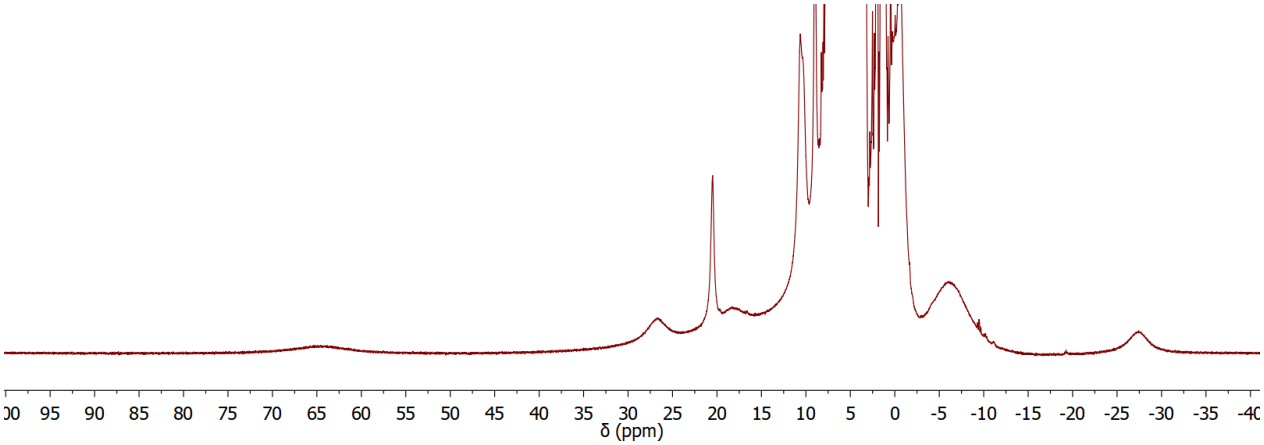

Figure S14 ^{1}H NMR spectrum of [(P_2P^{Ph})Fe(N_2)][K(18-crown-6)] (**9**) in d_8-THF at room temperature

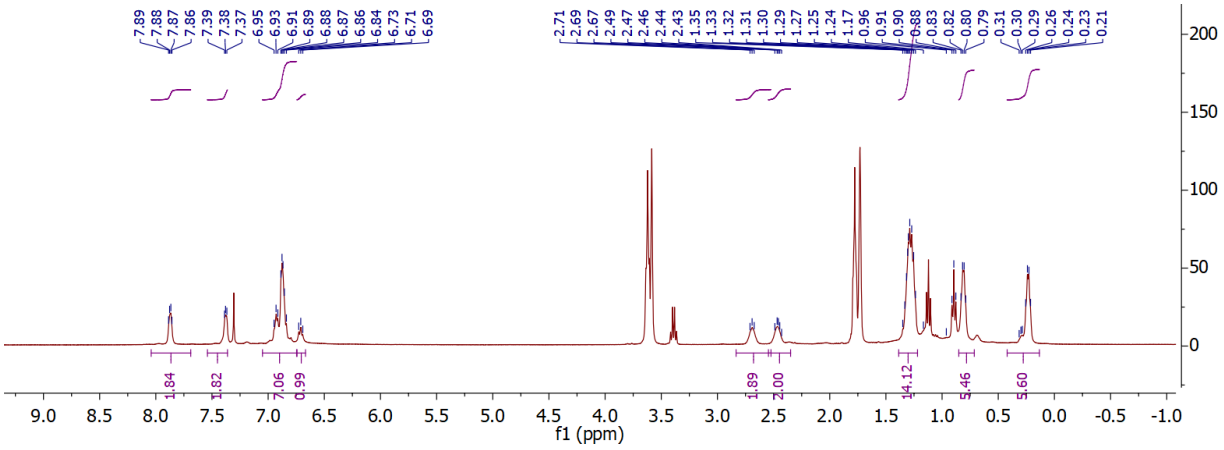

Figure S15 ^{1}H NMR spectrum of [(P_2P^{Ph})Fe(N_2)][K_2(THF)$_3$] (**10**) in d_8-THF at room temperature

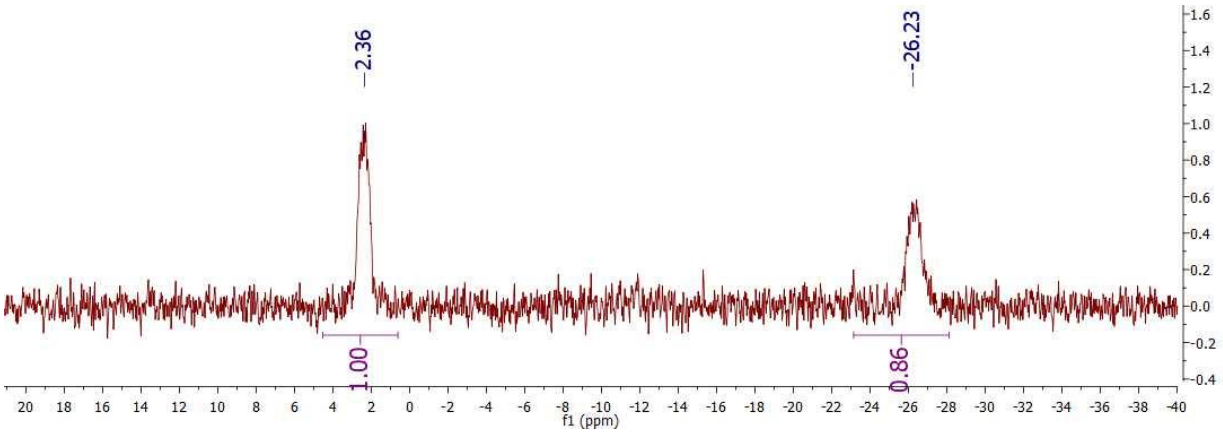

Figure S16 ^{15}N NMR spectrum of $[(P_2P^{Ph})Fe(N_2)][K_2(THF)_3]$ in d_8-THF at room temperature

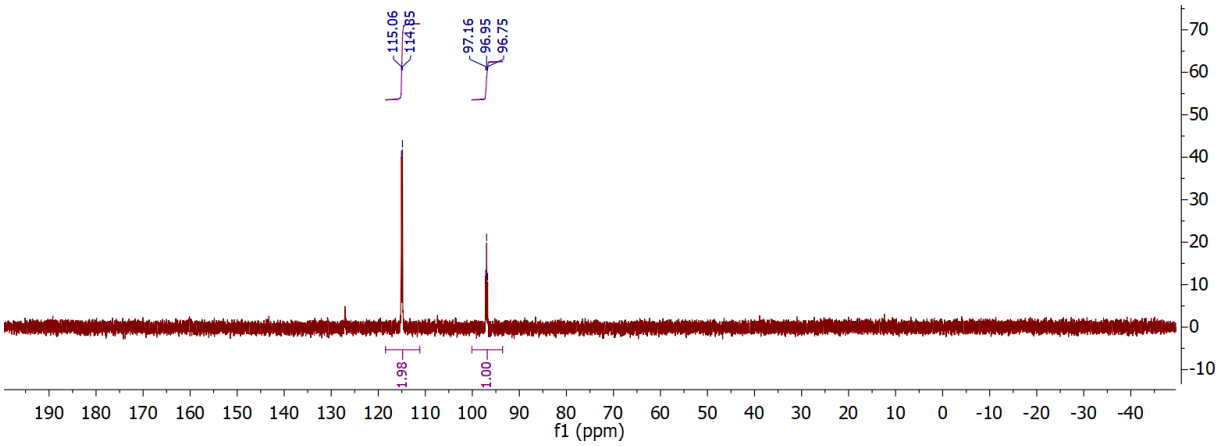

Figure S17 ^{31}P NMR spectrum of $[(P_2P^{Ph})Fe(N_2)][K_2(THF)_3]$ in d_8-THF at room temperature

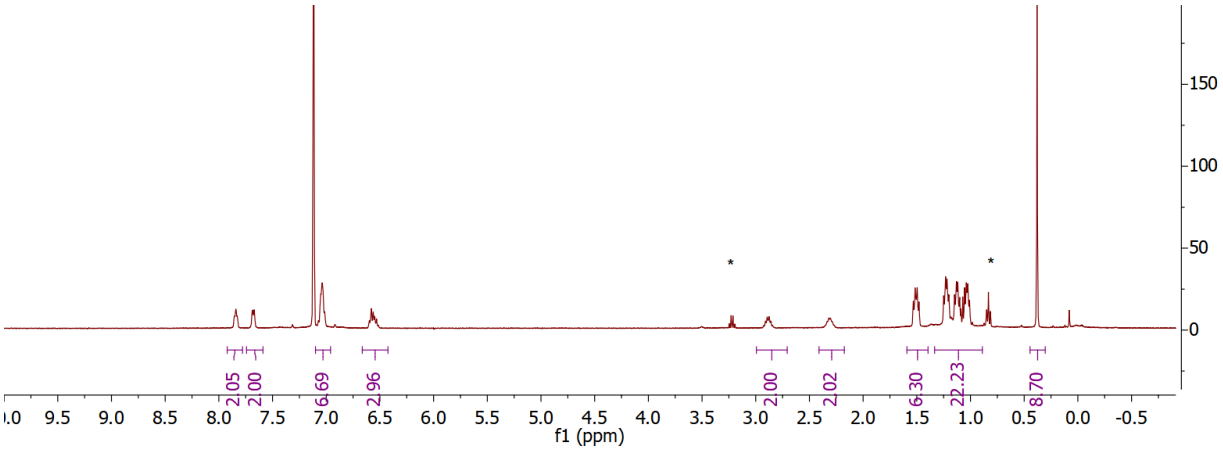

Figure S18 ^{1}H NMR spectrum of $[(P_2P^{Ph})Fe(NNTMS)]K$ in C_6D_6 at room temperature. The peaks labeled with a star correspond to residual diethyl ether.

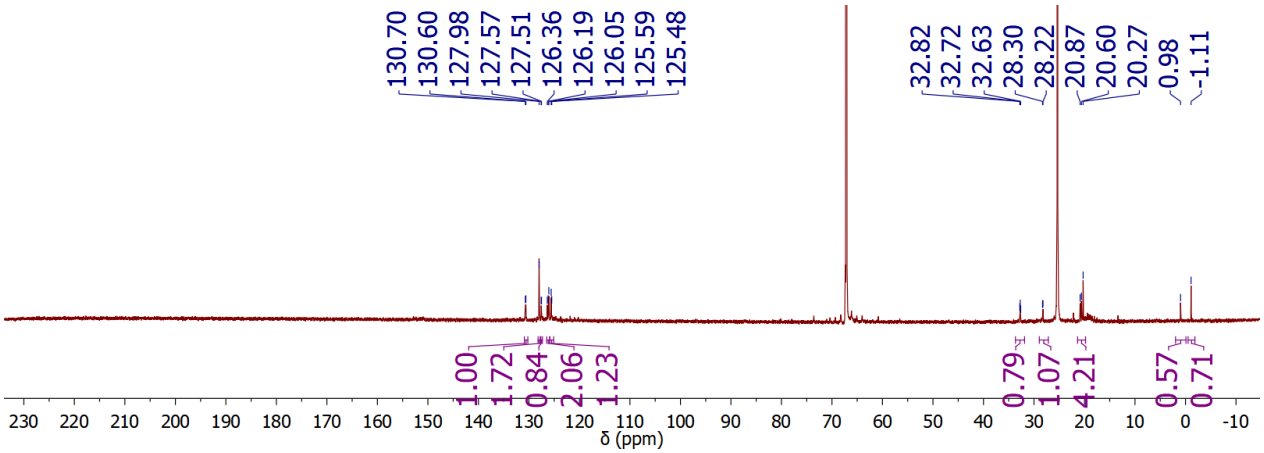

Figure S19 ^{13}C NMR spectrum of [(P_2P^{Ph})Fe(NNSiMe$_3$)]K (**11**-NNSiMe$_3$) in THF at room temperature. The peaks labeled with a star correspond to residual diethyl ether.

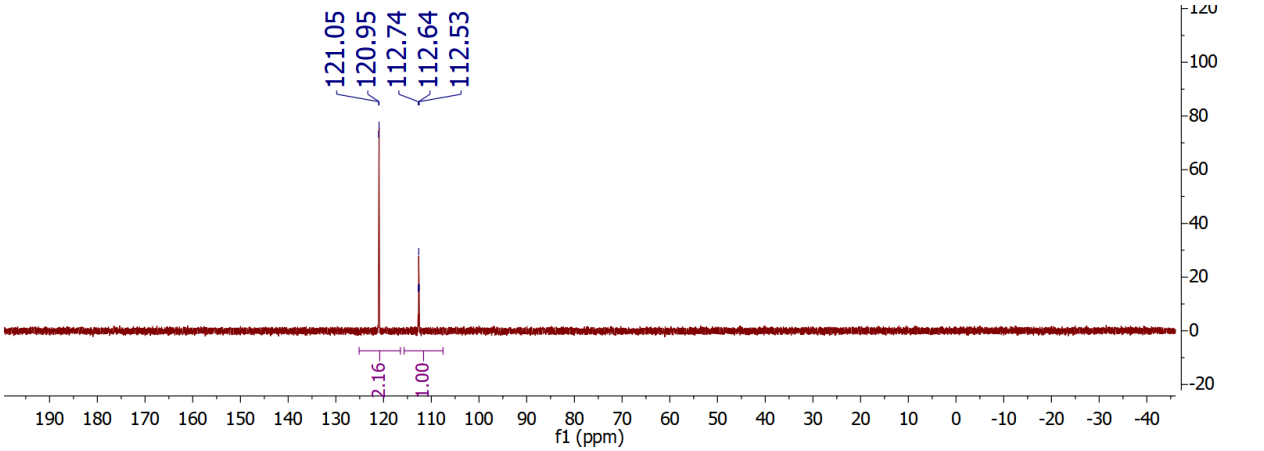

Figure S20 ^{31}P NMR spectrum of [(P_2P^{Ph})Fe(NNSiMe$_3$)]K (**11**-NNSiMe$_3$) in C_6D_6 at room temperature. The peaks labeled with a star correspond to residual diethyl ether.

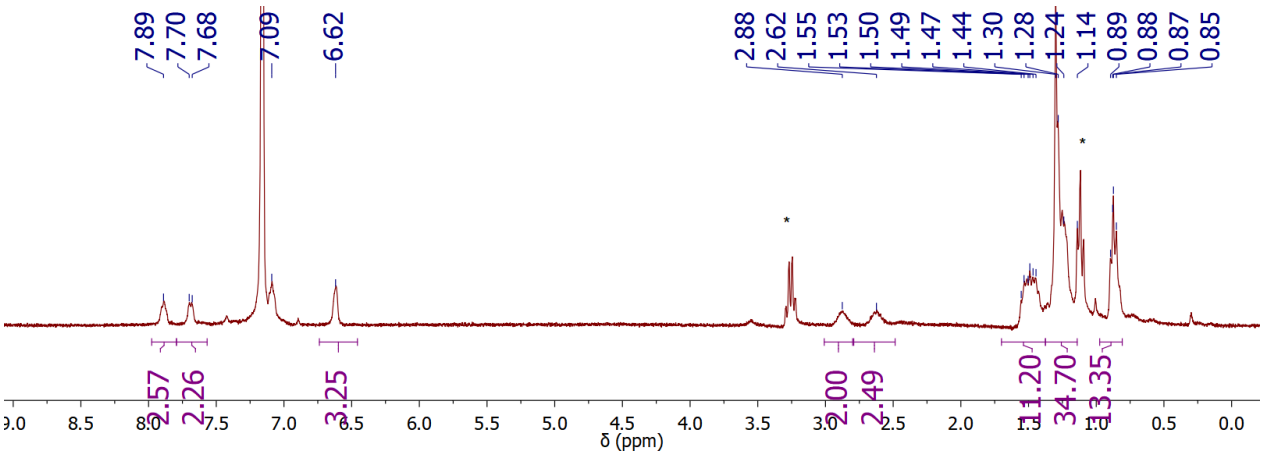

Figure S21 ^{1}H NMR spectrum of [(P_2P^{Ph})Fe(NNSi^{i}Pr$_3$)]K (**11**-NNSi^{i}Pr$_3$) in C_6D_6 at room temperature. The peaks labeled with a star correspond to residual diethyl ether.

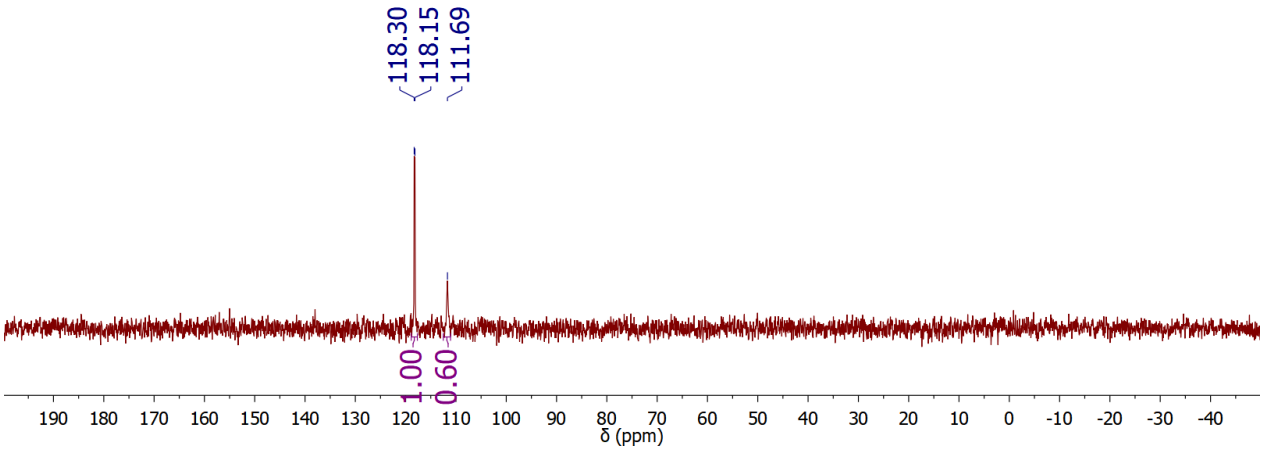

Figure S22 ^{31}P NMR spectrum of [(P_2P^{Ph})Fe(NNSi^{i}Pr$_3$)]K (**11**-NNSi^{i}Pr$_3$) in C_6D_6 at room temperature. The peaks labeled with a star correspond to residual diethyl ether.

NMR spectra of stoichiometric reactivity

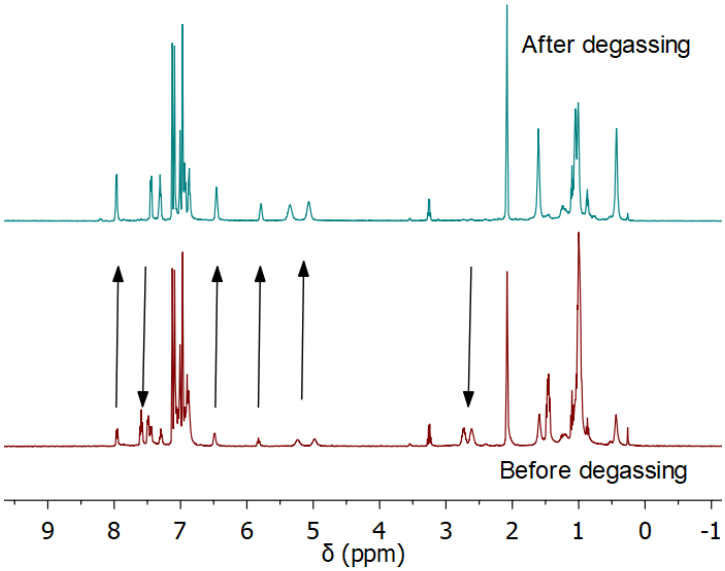

Figure S23 ^{1}H NMR spectra of **5** before and after evacuation displaying the disappearance of **5** and the increased intensity of **6**.

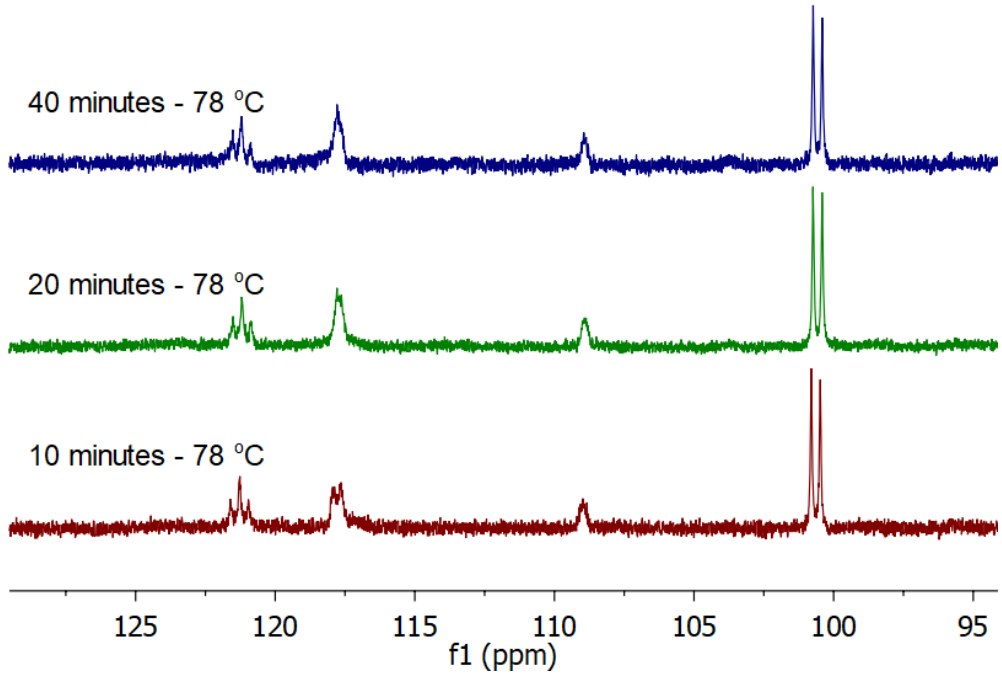

Figure S24 ^{31}P NMR spectra of the addition of H_2 to **5** before at −78 °C. The ratios between **5** and **2 (**indicated by a star) remain virtually the same upon storing the sample at −78 °C

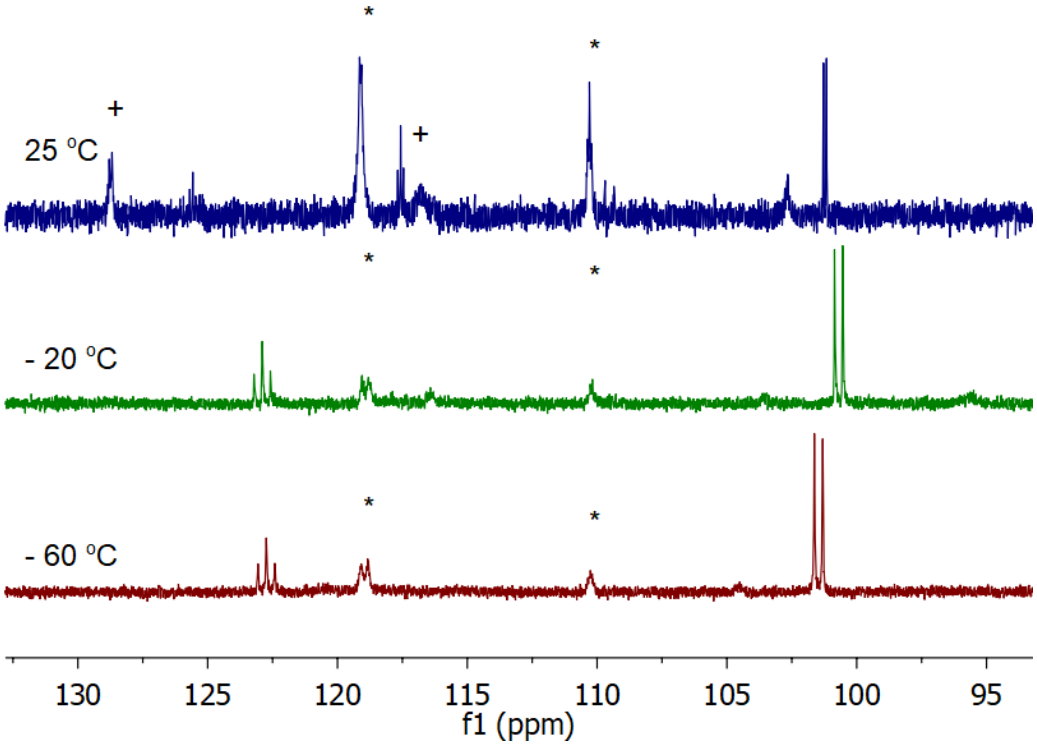

Figure S25 ^{31}P NMR spectra of the addition of H_2 to **5** before at various temperature. After the initial formation of **2** (indicated by a star), no appreciable reactivity was observed until the sample was warmed above −20 °C and a rapid change was observed at room temperature. The peaks labeled with (+) are likely due to the formation of "$(P_2P^{Ph})Fe(H_2)(H)_2$ as they disappear after addition of N_2.

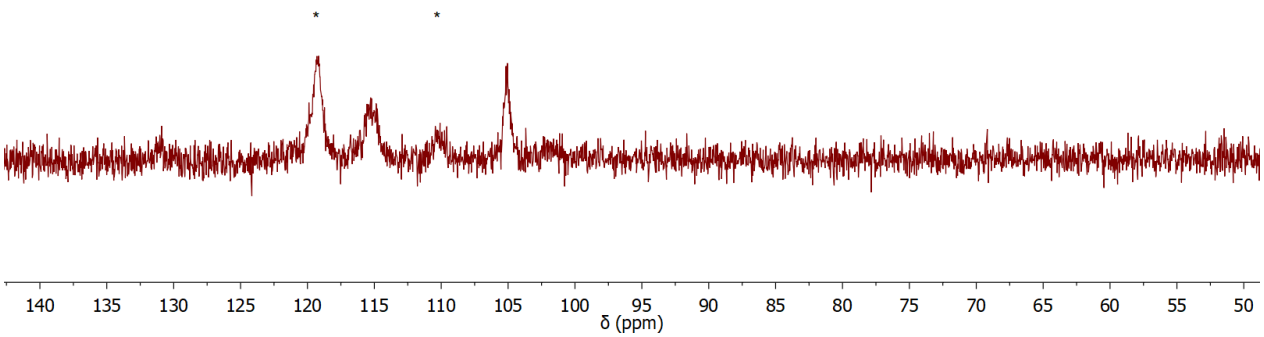

Figure S26 ^{31}P NMR spectrum of the addition of H_2 to **6** before at various temperature. Addition of H_2 results in the rapid formation of **2** (indicated by a star) and an unidentified species.

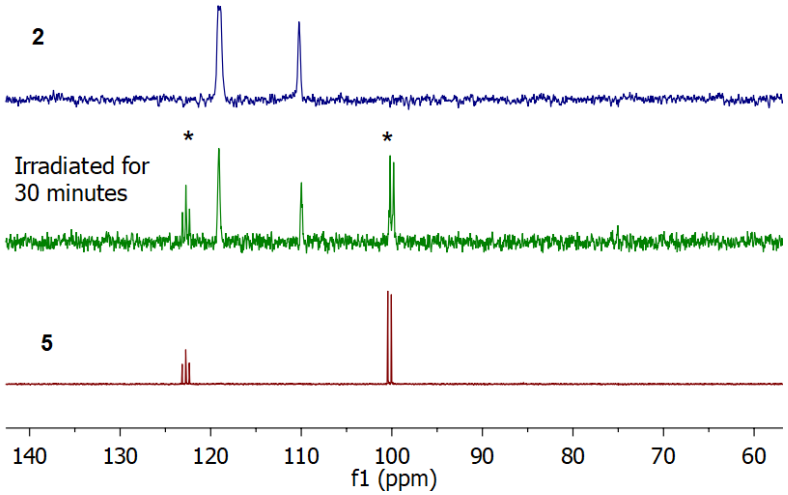

Figure S27 ^{31}P NMR spectrum of the irradiation of **2** which results in the formation of **5**.

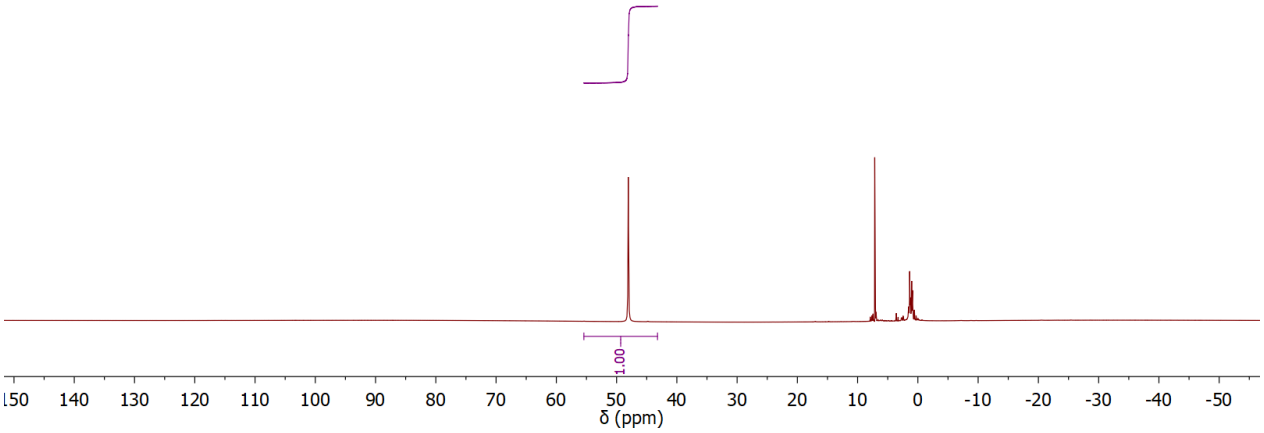

Figure S28 ^{1}H NMR spectrum of the oxidation of [(P_2P^{Ph})Fe(NNTMS)]K with [Cp^*_2Co][PF_6] at room temperature.

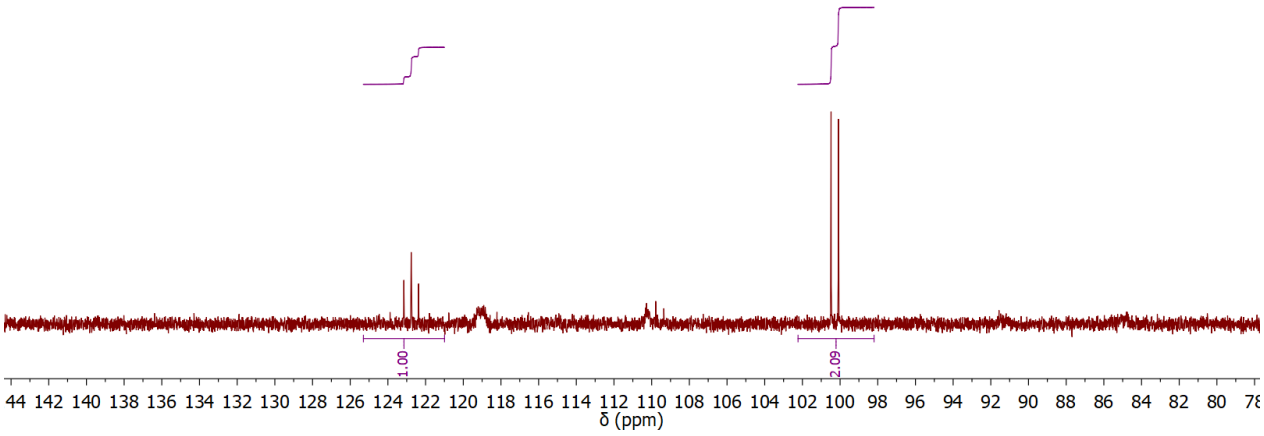

Figure S29 ^{31}P NMR spectrum of the oxidation of [(P_2P^{Ph})Fe(NNTMS)]K with [Cp*$_2$Co][PF_6] at room temperature with the characteristic features of **5**.

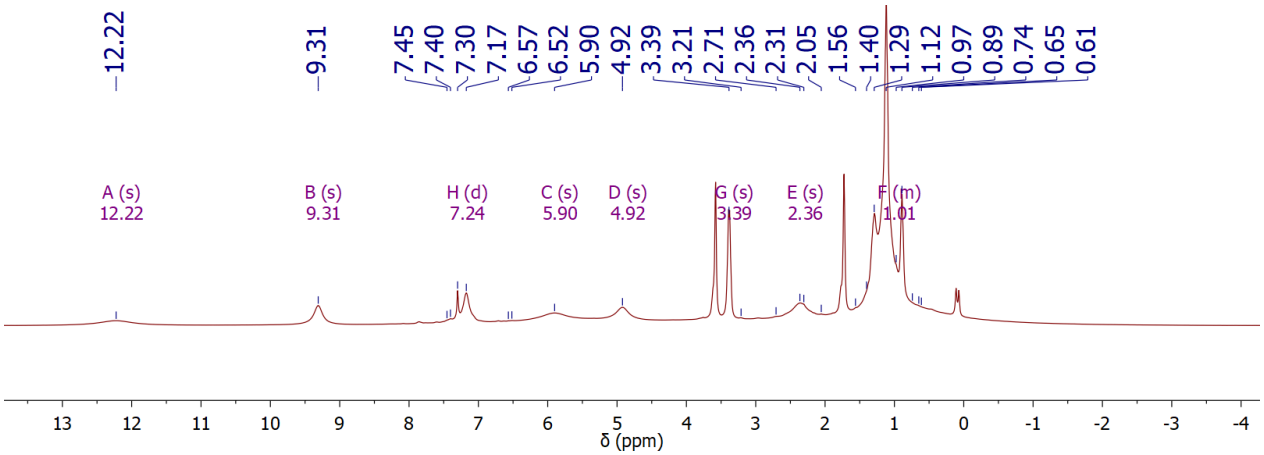

Figure S30 ^{1}H NMR spectrum of the oxidation of [(P_2P^{Ph})Fe(NNTiPS)]K with [Cp*$_2$Co][PF_6]

Fitting VT NMR data

The chemical shifts of the NMR active nuclei in **6** can be fit to a general equation accounting for the population of an excited state with equation S1:

$$\delta = \delta_o + \frac{B * (e^{\frac{2J}{kT}} + 5e^{\frac{6J}{kT}})}{(1 + 3e^{\frac{2J}{kT}} + 5e^{\frac{6J}{kT}}) * T} \quad \textbf{S1}$$

Herein, δ is the observed chemical shift for a nucleus at a given temperature, δ_o is the chemical shift of that atom in the ground state, B is a fitting constant, and 2J and 6J (as obtained for a Heisenberg–Dirac–VanVleck Hamiltonian in the notation $H = -2JS_1 \cdot S_2$) corresponds to the energy difference between the singlet and triplet, or the singlet and quintet states respectively. The theoretical framework for the use of this equation is described by Pfirrman *et al*.[9] Similar estimations of singlet–triplet gaps have been estimated for various systems.[9–13] One should note that such a large singlet triplet splitting (corresponding to a thermal energy of E/*k* = 2717 K) can be hardly detected by usual static magnetic susceptibility measurements as the thermal population of the triplet at 298 K is only about 0.034 % and the quintet is $6.7 \cdot 10^{-10}$ %.[9]

Overlap of three aromatic signals with toluene-d_8 hampered their analysis and therefore only ten out of the thirteen signals, expected in C_s symmetry, could be tracked reliably over the measured temperature range. The temperature dependent shift of these ten signals were simultaneously fit to equation S1 to give one value for J (−940 ± 9.4 cm^{-1}), ten chemical shifts corresponding to the ground state and ten fitting constants. The obtained fitting parameters are summarized in Table S1. As expected, the chemical shifts observed at 201 K are close to those determined for the ground state.

Table S1 Fit parameters for the chemicals shift of **6**

δ (ppm) at 201 K	δ_o (ppm)	B (10^5)
7.73	7.76 ± 0.02	5.4 ± 0.7
7.53	7.54 ± 0.02	-2.3 ± 0.6
7.46	7.51 ± 0.02	-26.9 ± 2.3
6.95	7.84 ± 0.02	-32.5 ± 2.7
2.49	2.41 ± 0.02	68.1 ± 5.7
1.83	1.73 ± 0.03	93.3 ± 7.7
1.38	1.35 ± 0.02	7.2 ± 0.8
1.31	1.24 ± 0.02	-3.9 ± 0.6
0.95	0.92 ± 0.02	2.8 ± 0.6
0.68	0.71 ± 0.02	-7.1 ± 0.8

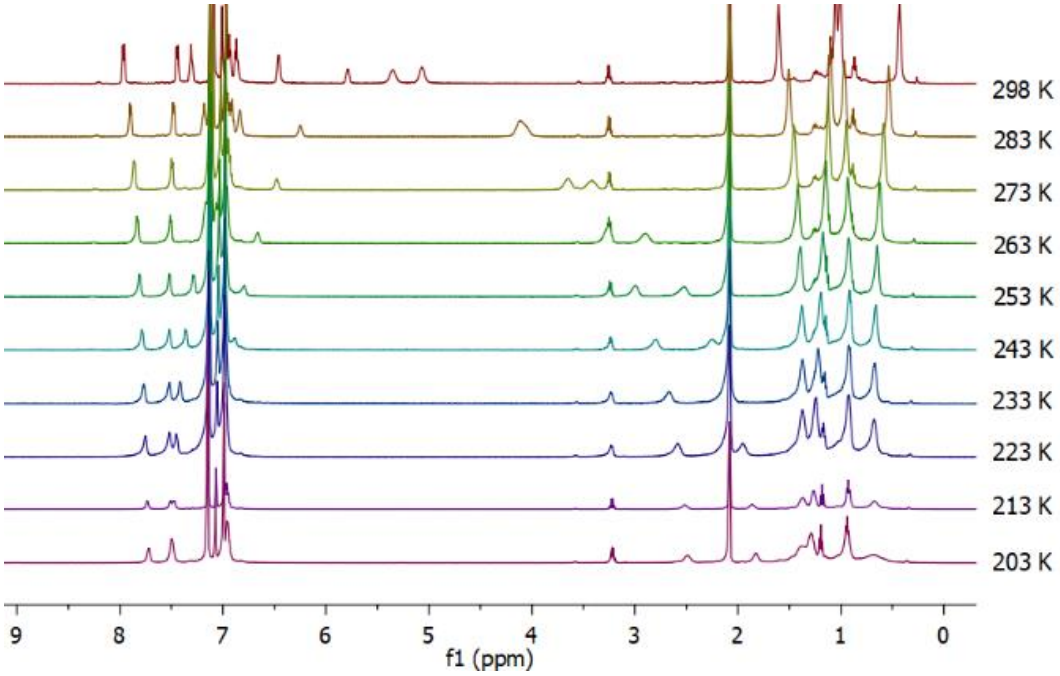

Figure S31 Selected ^{1}H NMR spectra of **6** in *d*8-toluene plotted at various temperatures

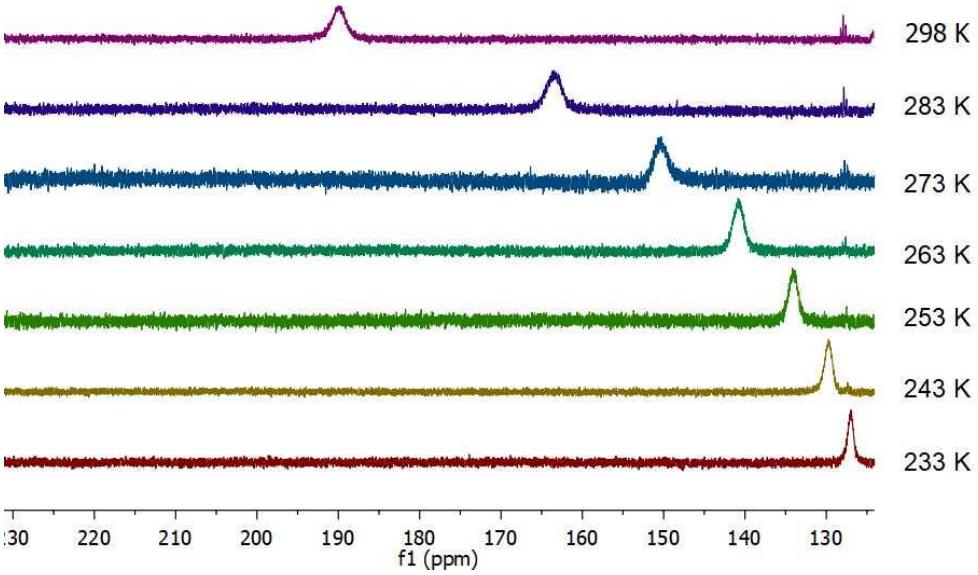

Figure S32 Selected ^{31}P NMR spectra of **6** *d*8-toluene plotted at various temperatures

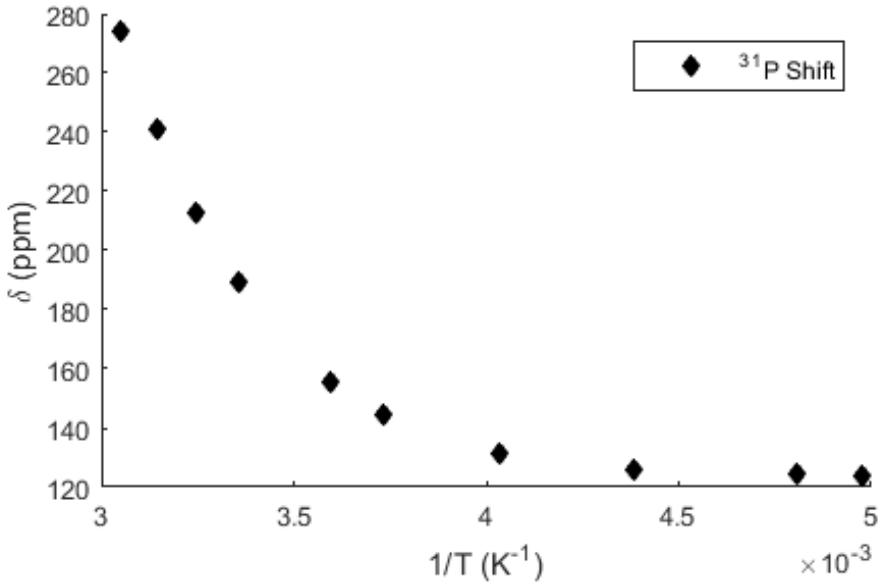

Figure S33 ^{31}P NMR chemical shifts of **6** plotted as a function of 1/T

IR Spectra

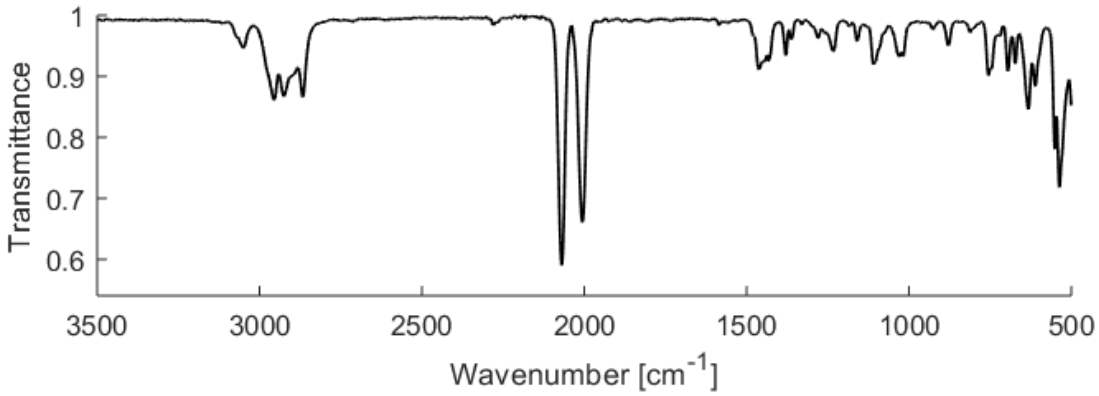

Figure S34 IR spectrum of $(P_2P^{Ph})Fe(N_2)_2$ (**5**) (thin-film from C_6D_6 solution)

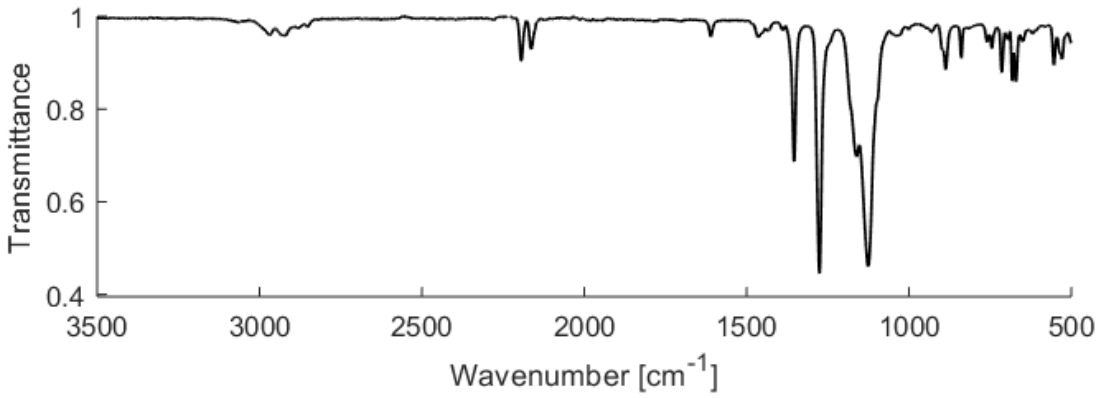

Figure S35 IR spectrum of $[(P_2P^{Ph})Fe(N_2)_2(H)][BAr^F]$ (**7**) (thin-film from *d*8-THF solution)

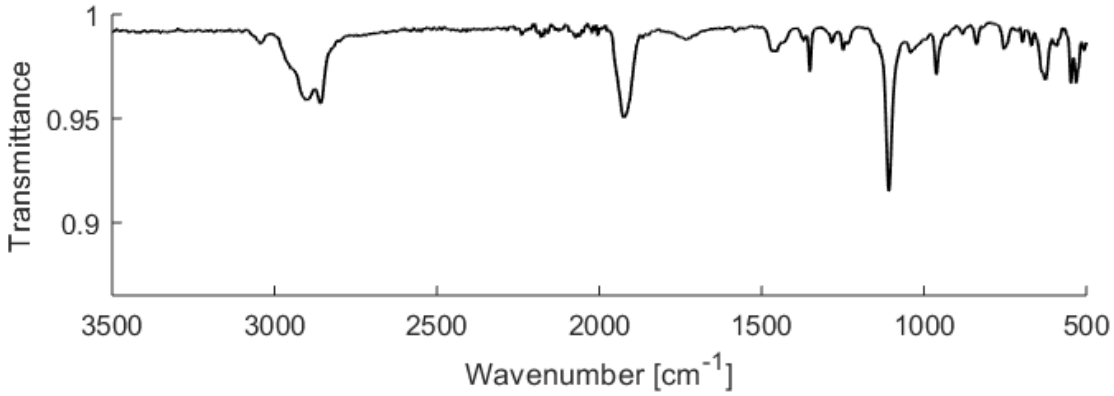

Figure S36 IR spectrum of $[(P_2P^{Ph})Fe(N_2)(H)][K(18\text{-crown-6})]$ (**8**) (thin-film from *d*8-THF solution)

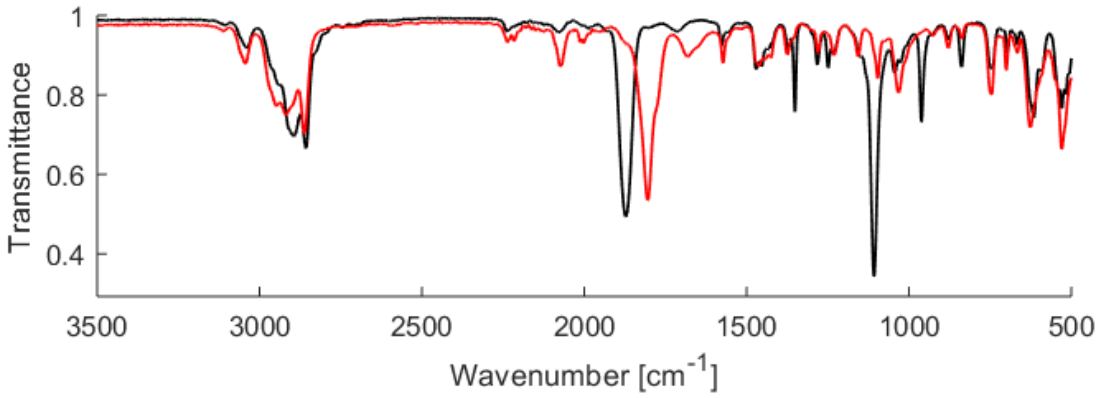

Figure S37 IR spectrum of [(P_2P^{Ph})Fe(N_2)][K(18-crown-6)] (**9**) in black (thin-film from *d*8-THF solution) and the spectrum of [(P_2P^{Ph})Fe(N_2)][K(THF)$_x$] recorded of a crude mixture before the addition of 18-crown-6

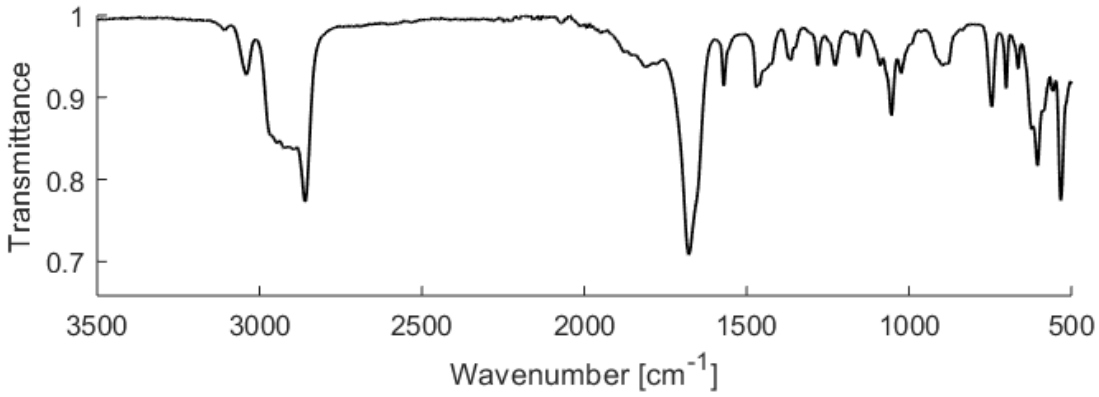

Figure S38 IR spectrum of [(P_2P^{Ph})Fe(N_2)][K_2(THF)$_3$] (**10**) (thin-film from THF solution)

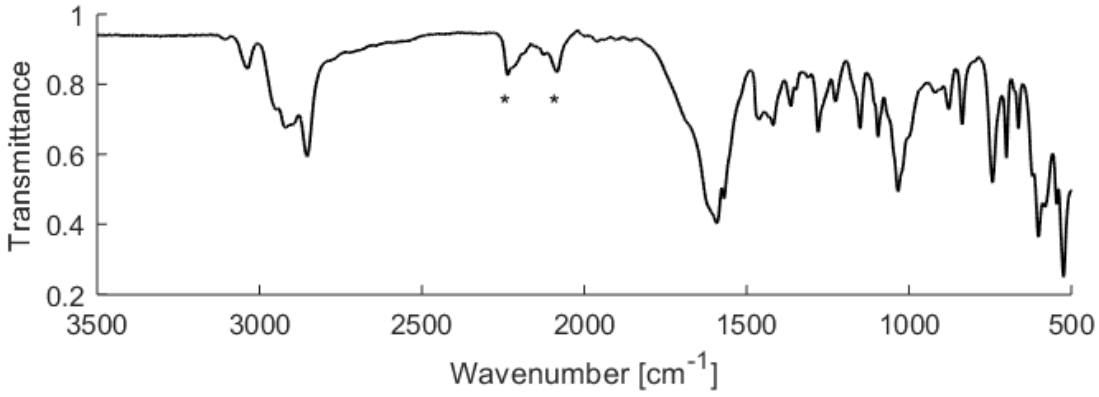

Figure S39 IR spectrum of [(P_2P^{Ph})Fe($^{15}N_2$)][K_2(THF)$_3$] (**10**) (thin-film from *d*8-THF solution). Bands marked with a star correspond to *d*8-THF

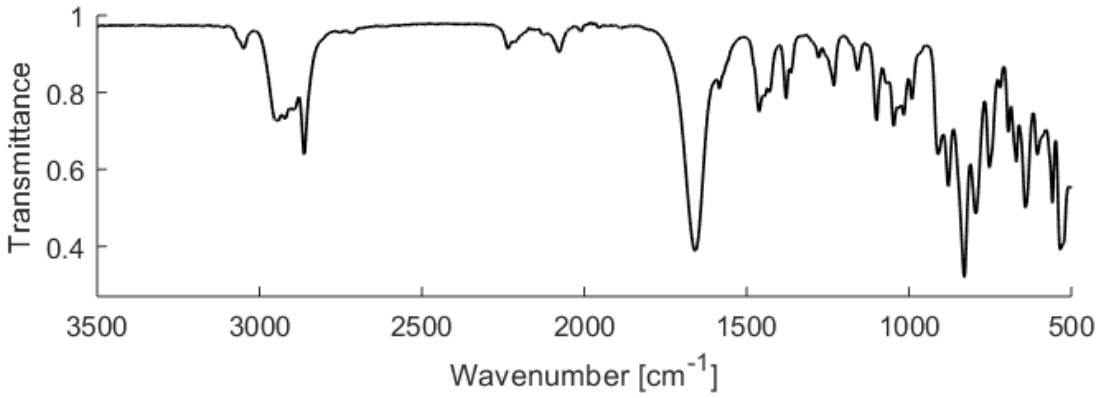

Figure S40 IR spectrum recorded after the irradiation of (P_2P^{Ph})Fe(NNSi^{i}Pr$_3$) (**12-NNSi^{i}Pr$_3$**) (thin-film from *d*8-THF solution)

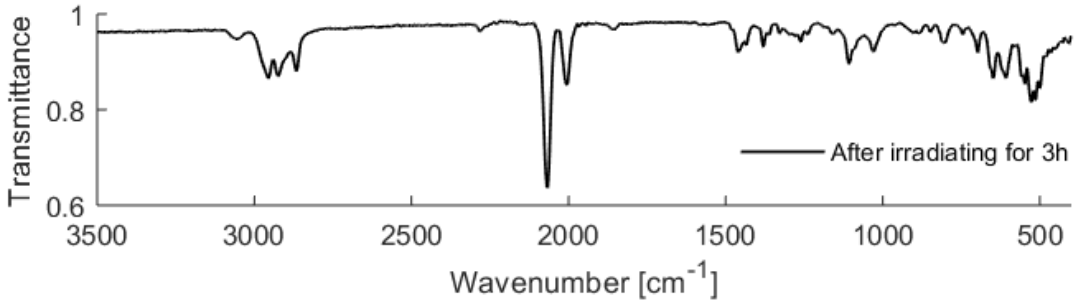

Figure S41 IR spectrum recorded after the irradiation of (P_2P^{Ph})Fe(N_2)(H_2) (**2**) (thin-film from C_6D_6 solution)

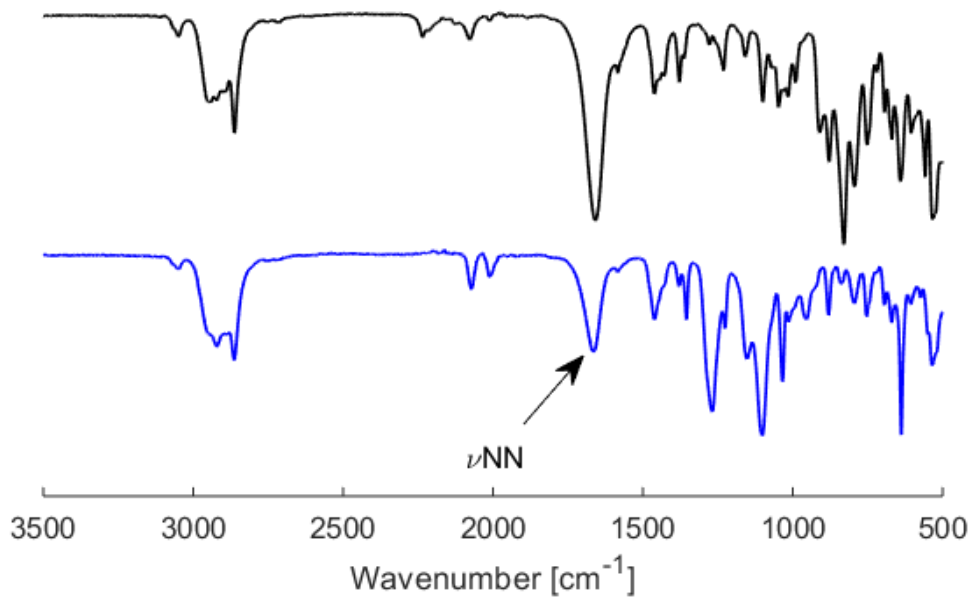

Figure S42 Thin-film IR spectra of **12**-NNSi^{i}Pr$_3$ with *ν*NN in black and the addition of ^{i}Pr$_3$SiOTf to **9** in blue.

Cyclic Voltammograms

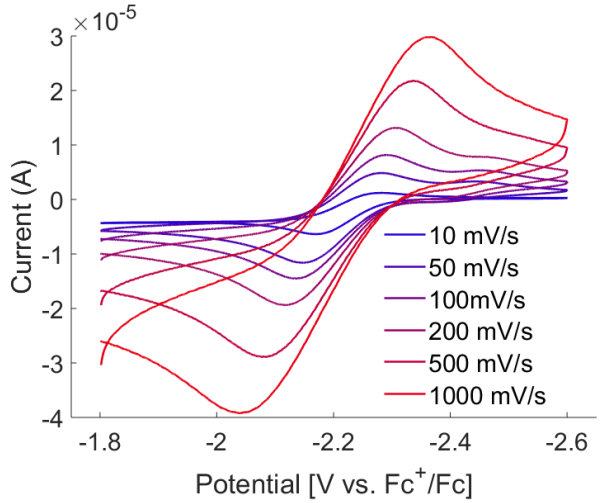

Figure S43 (Top) Scan rate dependence of the wave observed at −2.4 V in the cyclic voltammogram of [(P_2P^{Ph})Fe(N_2)(H)][K(18-crown-6)] (**8**) scanning in the anodic direction.

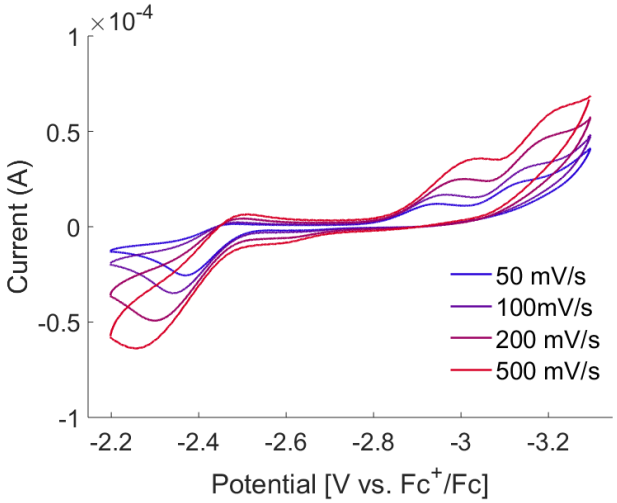

Figure S44 (Top) Cyclic voltammogram of [(P_2P^{Ph})Fe(N_2)][K(18-crown-6)] (**9**) scanning in the cathodic direction.

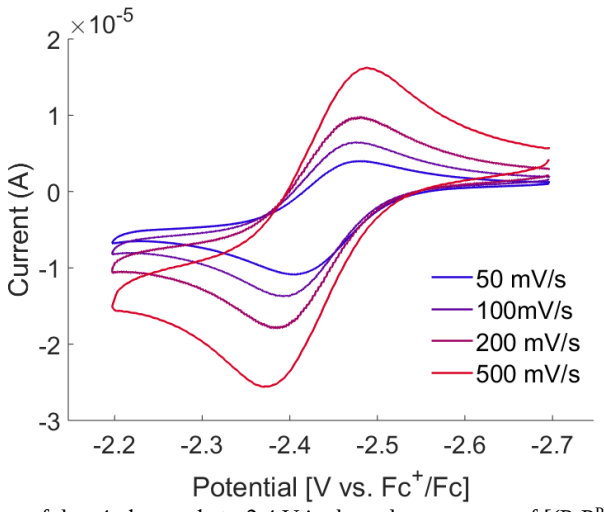

Figure S45 Scan rate dependence of the r4 observed at −2.4 V in the voltammogram of [(P_2P^{Ph})Fe(N_2)][K(18-crown-6)] (**9**).

EPR Spectra

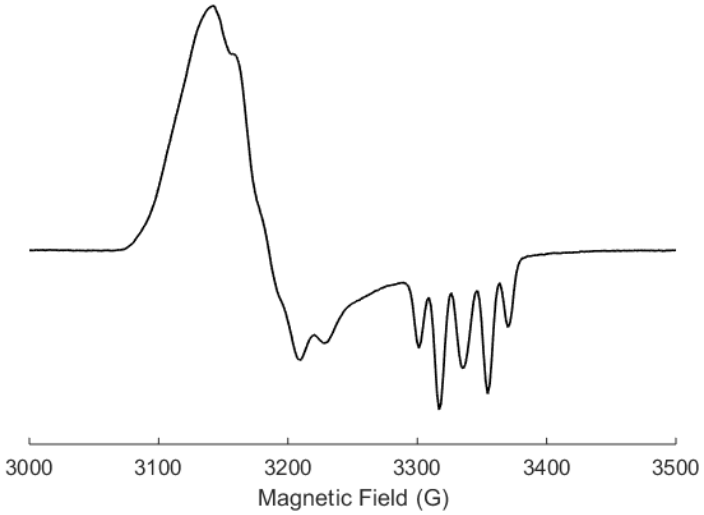

Figure S46 EPR spectrum of [(P_2P^{Ph})Fe(N_2)][K(18-crown-6)] in 2-MeTHF, at 77 K, microwave frequency 9.39 GHz, microwave power 6.47 mW.

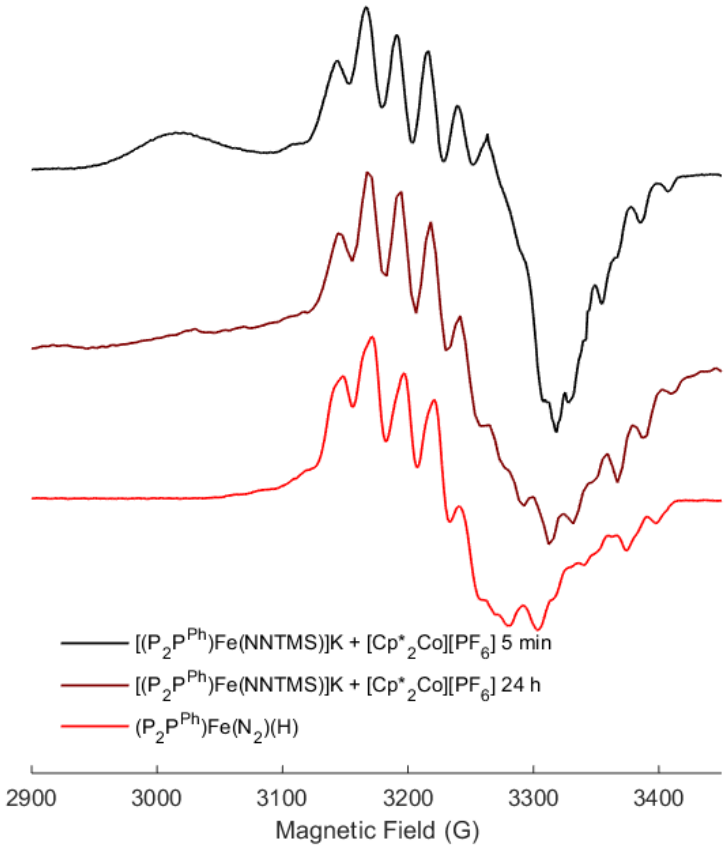

Figure S47 EPR spectra of the oxidation of $[(P_2P^{Ph})Fe(NNSiMe_3)]K$ with $[Cp^*_2Co][PF_6]$ in THF at different time points and the EPR spectrum of $(P_2P^{Ph})Fe(N_2)(H)$

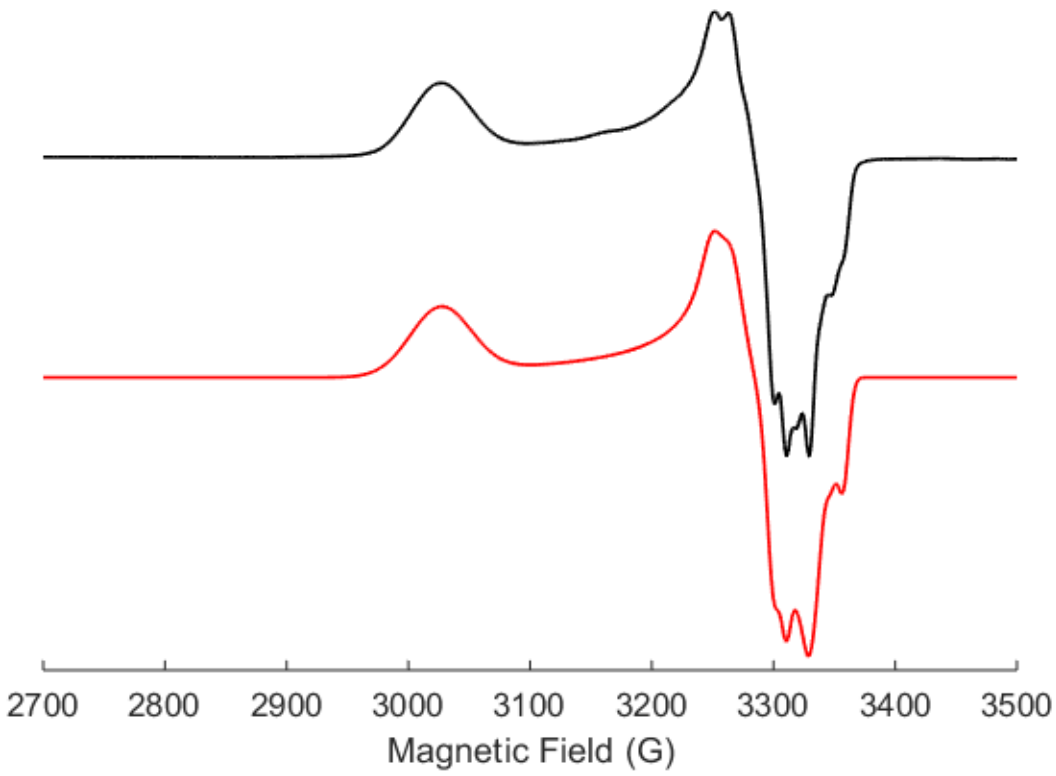

Figure S48 EPR spectrum of the oxidation of [(P_2P^{Ph})Fe(NNSi^{i}Pr$_3$)]K (**11**-NNSi^{i}Pr$_3$) and [Cp*$_2$Co][PF_6] resulting in the formation of (P_2P^{Ph})Fe(NNSi^{i}Pr$_3$) (**12**-NNSi^{i}Pr$_3$) andd fit of the spectrum in respectively black and red. Simulation parameters: g = [2.213 2.041 2.012], P = [0 40.3 57.1] P = [0 40.3 75.0] P = [0 69.4 29.0] Hstrain = [1180 50 30]

Mössbauer Spectra

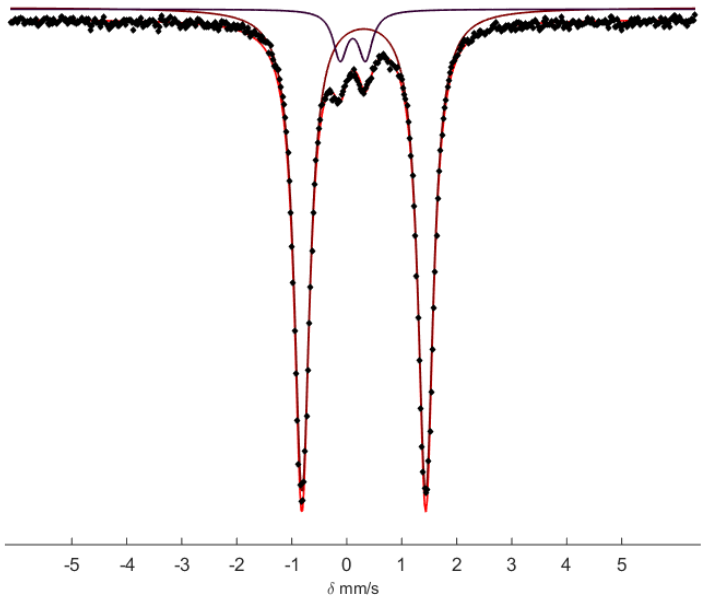

Figure S49 Mössbauer spectrum collected of $(P_2P^{Ph})Fe(N_2)_2$ (**5**) at 80 K Raw data shown as black points, overall simulation as a red line. The major species, **5**, in purple is fit as a doublet (δ = 0.31 mm s^{-1}, ΔE_Q = 2.16 mm s^{-1}). The minor species (~ 5%) in blue was fit as a doublet (δ = 0.10 mm s^{-1}, ΔE_Q = 0.45 mm s^{-1})

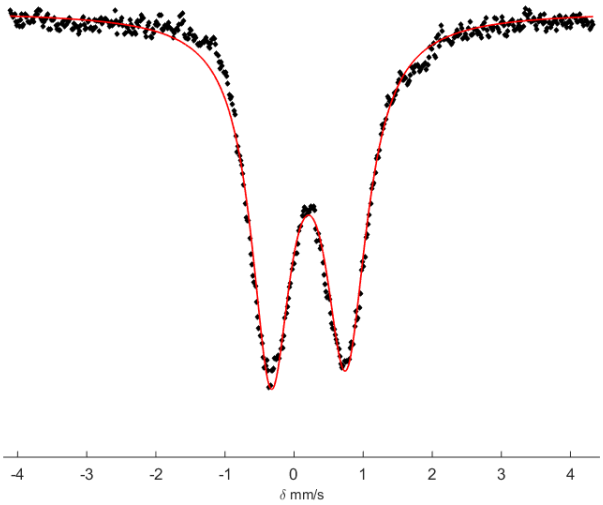

Figure S50 Mössbauer spectrum collected of $[(P_2P^{Ph})Fe(N_2)_2(H)][BAr^F{}_4]$ (**7**) at 80 K Raw data shown as black points, overall simulation as a red line. δ = 0.21 mm s^{-1}, ΔE_Q = 1.08 mm s^{-1}

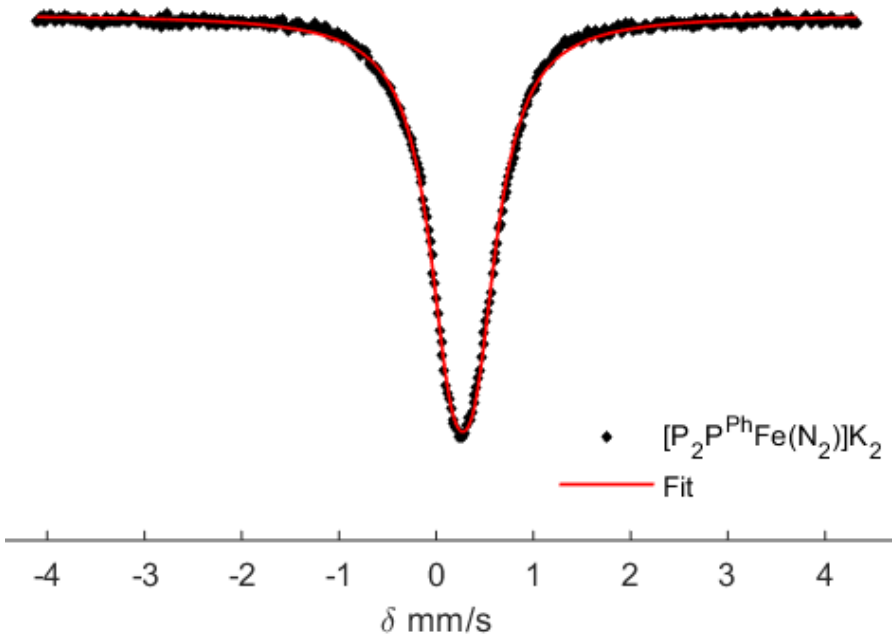

Figure S51 Mössbauer spectrum collected of [(P_2P^{Ph})Fe(N_2)]K_2(THF)$_3$] (**10**) at 80 K Raw data shown as black points and simulated spectrum in red (δ = 0.27 mm s^{-1}, ΔE_Q = 0.26 mm s^{-1}).

UV-vis Spectra

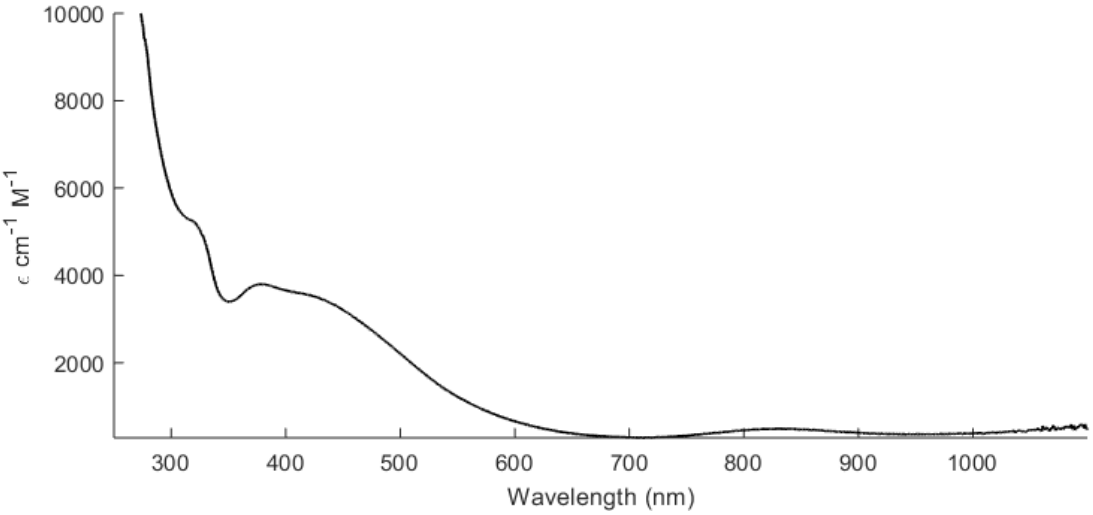

Figure S52 UV-visible spectrum of (P_2P^{Ph})FeBr (**4**) THF, 293 K)

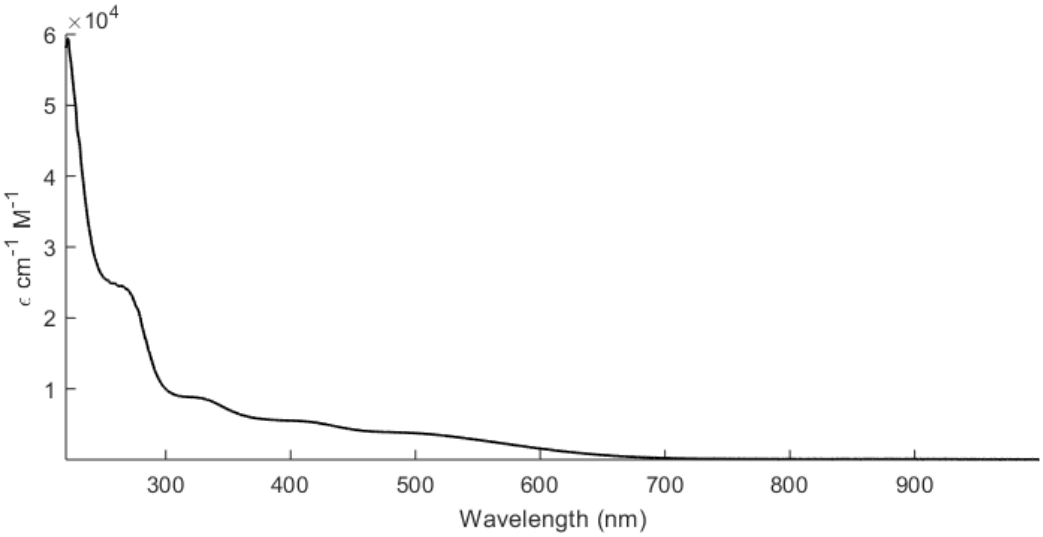

Figure S53 UV-visible spectrum of $(P_2P^{Ph})Fe(N_2)_2$ (**5**) (Et_2O, 293 K)

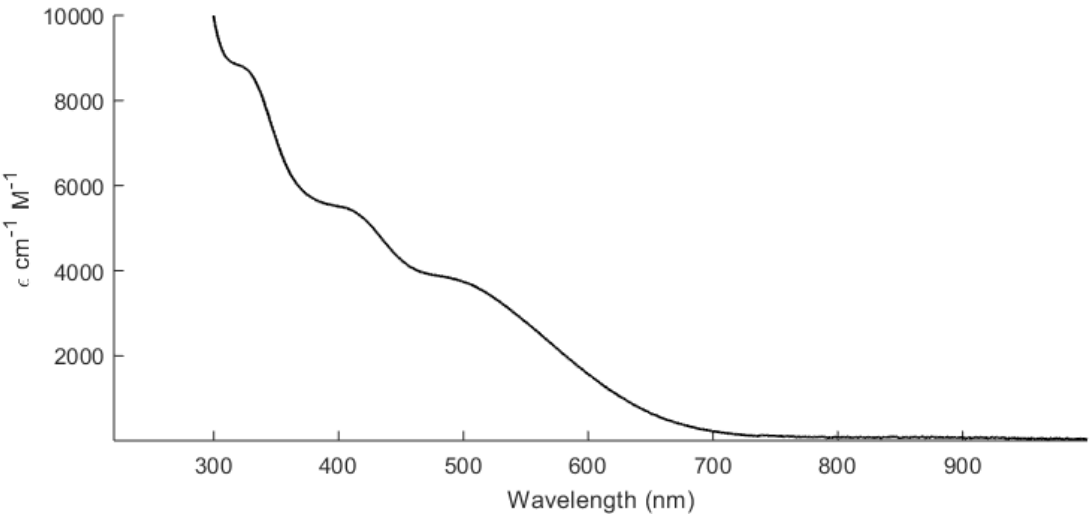

Figure S54 UV-visible spectrum of $(P_2P^{Ph})Fe(N_2)_2$ (**5**) (Et_2O, 293 K)

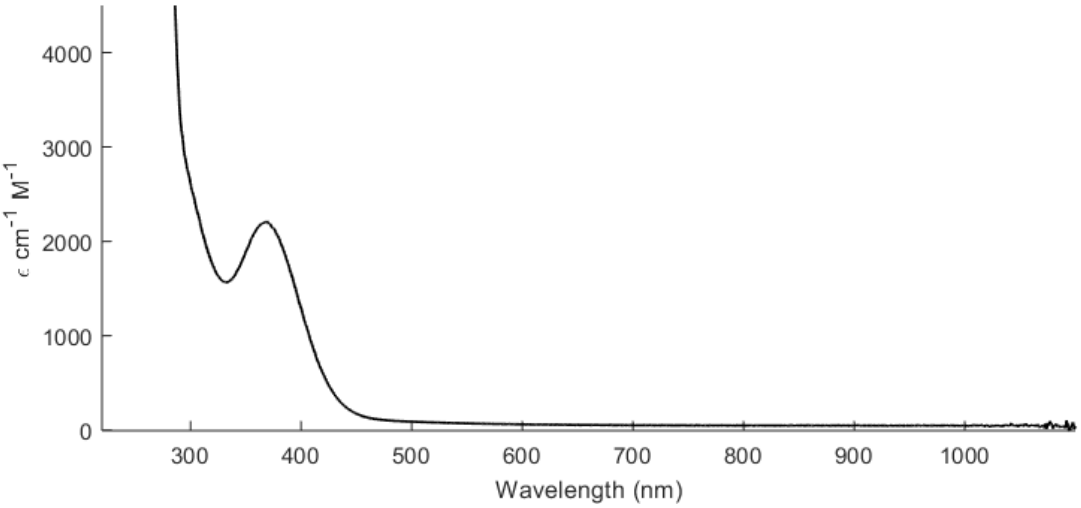

Figure S55 UV-visible spectrum of [(P_2P^{Ph})Fe(N_2)$_2$(H)][BAr^F_4] (**7**) (Et_2O, 293 K)

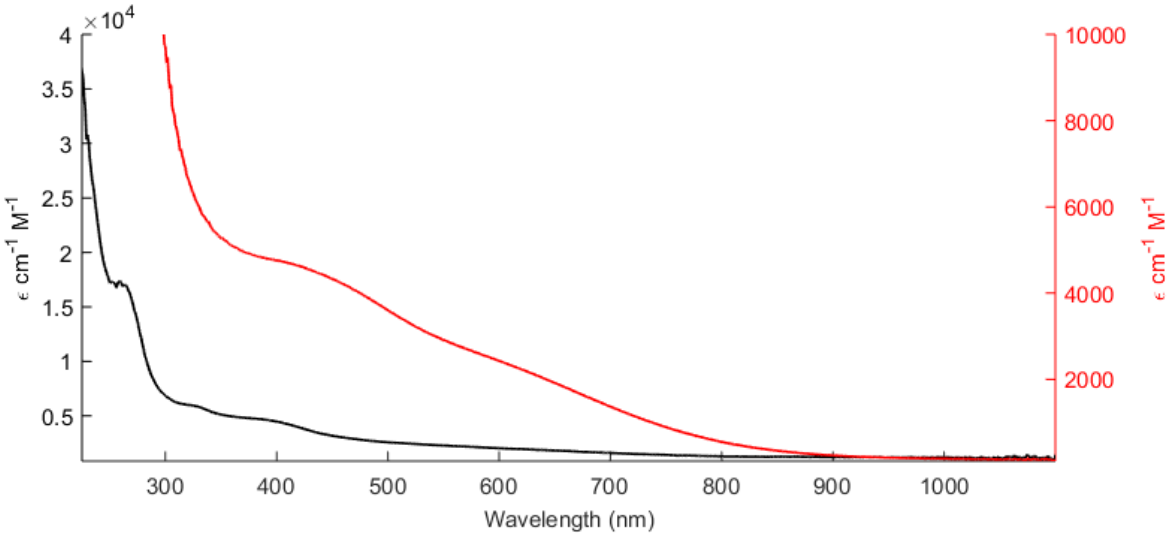

Figure S56 UV-visible spectrum of [(P_2P^{Ph})Fe(N_2)(H)][K(18-crown-6)] (**8**) (2-MeTHF, 293 K). Black trace corresponds to the left axis scale, while the red trace corresponds to the right axis scale.

Catalytic experiments

Standard NH3 Generation Reaction Procedure. All solvents were stirred with Na/K for ≥1 hour and filtered through alumina prior to use. In a nitrogen-filled glovebox, a stock solution of the catalyst in THF (6.8 mM) was prepared. (Note: a fresh stock solution was prepared for each experiment and used immediately.) An aliquot of this stock solution (90 or 270 μL, 0.6 or 1.82 μmol) was added to a Schlenk tube and evaporated to dryness under vacuum to give a thin film of the precatalyst. The tube was allowed to cool to 77 K in the glovebox cold well. To the cold tube was added a solution of $[H(OEt_2)_2][BAr^F{}_4]$ (93 mg, 0.092 mmol) in Et_2O (0.5 mL). This solution was allowed to freeze before the vial which contained the $HBAr^F{}_4$ was rinsed with an additional 0.5 mL of Et_2O and added to the tube. After the acid layer froze, a suspension of KC_8 (15 mg, 0.111 mmol) in 0.5 mL of Et_2O (1.2 equiv. relative to $[H(OEt_2)_2][BAr^F{}_4]$) was added to the cold tube. A stir bar was added to the tube and the tube sealed with a Teflon screw-valve. The temperature of the system was allowed to equilibrate for 5 minutes. The Schlenk tube was passed out of the box into a liquid N_2 bath and transported to a fume hood. The reaction vessel was subsequently transferred to a dry ice/acetone bath where it thawed to -78 °C and was allowed to stir for at least 1 hour. The tube was then warmed to room temperature while stirring and subsequently stirred at room temperature for 5 minutes.

Standard NH3 Generation Reaction with Hg Lamp Photolysis Procedure. Preparation of the Schlenk tube containing reactants was performed as described for runs without light. The cold reaction vessel was transferred to a dry ice/isopropanol bath which was positioned under a Hg lamp and turned on 1 minute prior to transfer of the Schlenk tube to the bath. The entire reaction apparatus was surrounded by aluminum foil and the reaction vessel was stirred for at least 1 hour before the Hg lamp was turned off and the Schlenk tube was allowed to warm to room temperature with stirring and stirred at room temperature for 5 minutes.

Ammonia Quantification. The catalytic reaction mixture was cooled to 77 K and allowed to freeze. The reaction vessel was opened to the atmosphere and to the frozen solution was slowly added a fourfold excess (with respect to acid) solution of a NaO*t*Bu in MeOH (0.25 M) over 1–2 minutes. The solution was allowed to freeze, then the tube was sealed, evacuated and allowed to warm to room temperature and stirred at room temperature for 10 minutes. An additional Schlenk tube was charged with HCl (3 mL of a 2.0 M solution in Et_2O, 6 mmol) to serve as a collection flask. The volatiles of the reaction mixture were vacuum transferred into the collection flask. After completion of the vacuum transfer, the collection flask was sealed and warmed to room temperature. Solvent was removed *in vacuo*, and the remaining residue dissolved in H_2O (1 mL) to make a stock solution that was used for ammonia quantification. An aliquot of this solution (20 μL) was then analyzed for the presence of NH_3 (present as NH_4Cl) by the indophenol method. Quantification was performed with UV−Vis spectroscopy by analyzing the absorbance at 635 nm.

Yields of Independent Catalytic Runs

Table S2 Results of individual runs using **4** at 150 equiv. acid loading with no Hg lamp irradiation.

Run	Absorbance	Equiv. NH_3/Fe	% Yield (Based of H^+)
A	0.017	0.86	1.7
B	0.022	0.63	1.3

Table S3 Results of individual runs using **5** at 50 equiv. acid loading with no Hg lamp irradiation.

Run	Absorbance	Equiv. NH_3/Fe	% Yield (Based of H^+)
A	0.401	5.09	30.6
B	0.399	5.06	30.4

Table S4 Results of individual runs using **5** at 150 equiv. acid loading with no Hg lamp irradiation.

Run	Absorbance	Equiv. NH_3/Fe	% Yield (Based of H^+)
A	0.171	6.40	12.8
B	0.152	5.66	11.3

Table S5 Results of individual runs using **5** at 150 equiv. acid loading with Hg lamp irradiation.

Run	Absorbance	Equiv. NH_3/Fe	% Yield (Based of H^+)
A	0.240	8.83	17.7
B	0.315	12.01	24.0
C	0.207	7.78	15.6

Table S6 Results of individual runs using **5** at 150 equiv. acid loading with one equiv. TBABr added.

Run	Absorbance	Equiv. NH_3/Fe	% Yield (Based of H^+)
A	0.055	1.88	3.8
B	0.072	2.55	5.1

Table S7 Results of individual runs using **5** with 150 equiv. Ph_2NH_2OTf with no Hg lamp irradiation.

Run	Absorbance	Equiv. NH_3/Fe	% Yield (Based of H^+)
A	0.019	0.51	1.0
B	0.018	0.46	0.9

General Procedure for Time-resolved H_2 Quantification: Inside of a nitrogen filled glovebox, the Fe precursor (**2** or **5**, 1.5 μmol) was added to a 300 mL Schlenk flask as a solution in THF, and subsequently deposited as a thin film in a Schlenk flask by removing the solvent in vacuo. To this flask was added solid $HBAr^F_4$ (0.23 mmol), KC_8 (0.28 mmol), and a stir bar. The flask was sealed with a septum at room temperature and subsequently chilled to -196 °C in the cold well of a nitrogen filled glovebox. Et_2O (3 mL) was added via syringe into the flask and completely frozen. The flask was passed out of the glovebox into a liquid N_2 bath, and subsequently thawed in a dry ice/acetone bath. The timer was set to zero as soon as the flask was transferred to the dry ice/acetone bath. The headspace of the reaction vessel was periodically sampled with a sealable gas sampling syringe (10 mL), which was immediately loaded into the GC, and analyzed for the presence of H_2(g). From these data, the percent H_2 evolved (relative to $HBAr^F_4$) was calculated, correcting for the vapor pressure of Et_2O and the removed H_2 from previous samplings. Each time course was measured from a single reaction maintained at −78 °C.

Entry	Fe precursor	Time	% Yield (Based of H^+)
A	**2**	0	0
B		5	25.9
C		25	70.7
.7D		60	74.4
E		120	72.6
F		1040	72.8
G	**5**	0	0
H		5	22.0
I		25	71.6
J		60	78.4
K		120	78.9
L		1040	79.5

General Procedure for the Preperation of Rapid-freeze-quenched Mössbauer Samples. The precatalyst was weighed into a vial (3 μmol) and dissolved in 0.5 mL Et_2O. The solvent was evaporated in a Schlenk tube to form a thin film of the precatalyst to which a stir bar was added. $HBAr^F_4$ (150 mg, 0.148 mmol) and KC_8 (24 mg, 0.178 mmol) are added as solids. The Schlenk tube was cooled to 77 K. To the cooled tube, 1 mL of Et_2O was added. The tube was then sealed with a Teflon screw tap and transferred to a prechilled cold well at − 78°C. The timer was set to zero as soon as the stir bar was freed from the thawing solvent. At the desired time, the tube was opened and the suspension was transferred to a Delrin cup pre-chilled to −78 °C using a pre-chilled pipette. The sample in the Delrin Cup was then rapidly frozen in liquid nitrogen. At this point, the frozen sample was taken outside the glovebox and mounted in the cryostat.

General Procedure for Fitting of Rapid-freeze-quench Mössbauer Samples. Simulations were constructed from the minimum number of quadrupole doublets required to attain a quality fit to the data (convergence of χ_R^2). Quadrupole doublets were constrained to be symmetric. It is known that the exact linewidths are sensitive to the particular sample, but the relative line breadth should be

fairly constant. Using the non-linear error analysis algorithm provided by WMOSS, the errors in the computed parameters are estimated to be 0.02 mm s-1 for δ and 2% for ΔEq. We additionally note that in these spectra the exact percentage contributions given do not represent exact percentages. Particularly for components that represent less than 10% of the overall spectrum, these values are subject to a high degree of uncertainty; however, all the included components are necessary to generate satisfactory fits of the data and therefore are believed to be present in the reaction mixtures.

Details of Individual of Rapid-freeze-quench Mössbauer Spectra

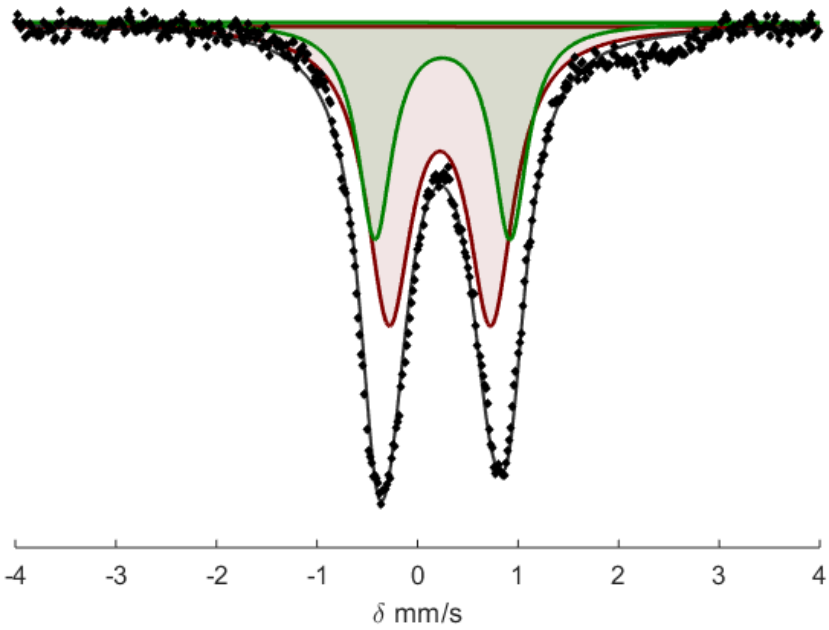

Figure S57 Mössbauer spectrum collected after rapid-freeze-quenching a catalytic reaction after 5 minutes using $(P_2P^{Ph})Fe(N_2)(H)_2$ (**2**) as precatalyst. Raw data shown as black points, overall simulation as a grey line, with components in green and red (see Table for parameters). The spectrum was collected at 80 K with a parallel applied magnetic field of 50 mT.

Fitting details for Figure S57: Various fits were attempted for the Mössbauer spectrum. The species could be fit with one quadruple doublet with a large linewidth. A better fit was obtained by fitting the spectrum with two quadrupole doublets with slightly different parameters. One of the species has parameters similar to $[(P_2P^{Ph})Fe(N_2)_2(H)][BAr^F{}_4]$ (**7**) The broad feature at 2 mm/s, present in various freeze quenched spectra, probably due to a magnetically split species, could not be fit.

Component	δ (mm s^{-1})	ΔE_Q (mm s^{-1})	Linewidths, Γ (mm s^{-1})	Relative area
A	0.22	1.01	0.54	0.63
B	0.24	1.34	0.41	0.37

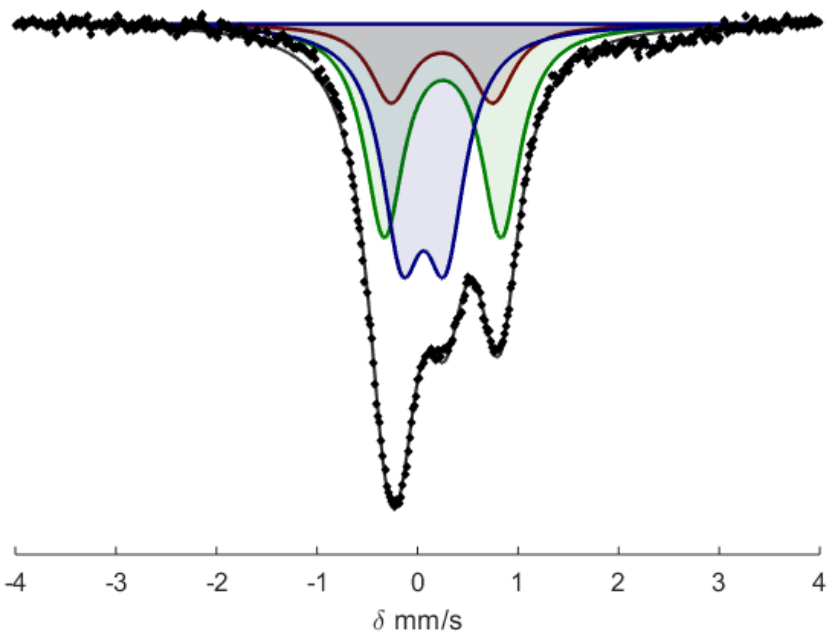

Figure S58 Mössbauer spectrum collected after rapid-freeze-quenching a catalytic reaction after 30 minutes using $(P_2P^{Ph})Fe(N_2)(H)_2$ (**2**) as precatalyst. Raw data shown as black points, overall simulation as a grey line, with components in green, blue and red (see Table for parameters). The spectrum was collected at 80 K with a parallel applied magnetic field of 50 mT.

Fitting details for Figure S58: Three quadrupole doublet were found to be necessary to obtain an adequate simulation. Two of the species could be fit with the same parameters as required for the freeze-quenched sample measured after 5 minutes. The remaining quadrupole doublet can be well simulated as $(P_2P^{Ph})Fe(N_2)(H_2)$.

Component	δ (mm s^{-1})	ΔE_Q (mm s^{-1})	Linewidths, Γ (mm s^{-1})	Relative area
A	0.22	1.01	0.50	0.15
B	0.25	1.16	0.46	0.42
C	0.06	0.43	0.48	0.43

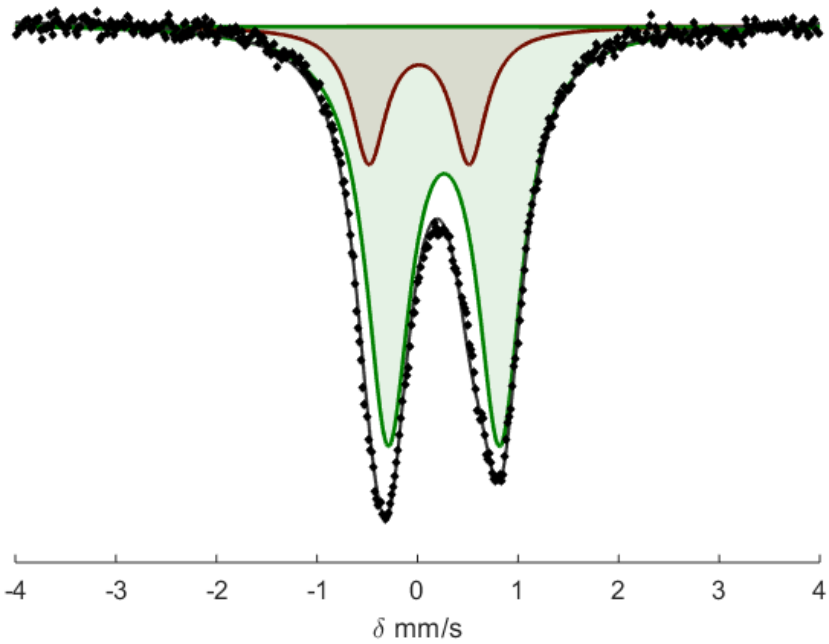

Figure S59 Mössbauer spectrum collected after rapid-freeze-quenching a catalytic reaction after 30 minutes using $(P_2P^{Ph})Fe(N_2)_2$ (**5**) as precatalyst. Raw data shown as black points, overall simulation as a grey line, with components in green, blue and red (see Table for parameters). The spectrum was collected at 80 K with a parallel applied magnetic field of 50 mT.

Fitting details for Figure S59 Mössbauer spectrum collected after rapid-freeze-quenching a catalytic reaction after 30 minutes using $(P2PPh)Fe(N2)_2$ (**5**) as precatalyst. Raw data shown as black points, overall simulation as a grey line, with components in green, blue and red (see Table for parameters). The spectrum was collected at 80 K with a parallel applied magnetic field of 50 mT. Various fits were attempted for the Mössbauer spectrum. The species could be fit with one quadruple doublet with a large linewidth. A better fit was obtained by fitting the spectrum with two quadrupole doublets with slightly different parameters. Of the several options, one gave a species with a similar isomer shift (0.26 mm/s) and quadrupole splitting (1.12 mm/s) as observed in the reactions with **2**.

Component	δ (mm s^{-1})	ΔE_Q (mm s^{-1})	Linewidths, Γ (mm s^{-1})	Relative area
A	0.16	1.00	0.41	0.20
B	0.26	1.12	0.52	0.80

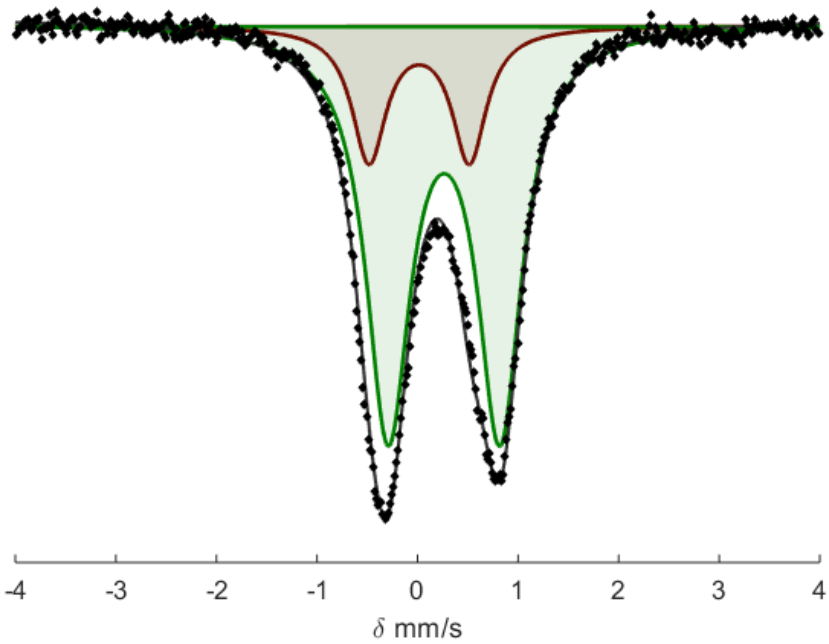

Figure S60 Mössbauer spectrum collected after rapid-freeze-quenching a catalytic reaction after 30 minutes using $(P_2P^{Ph})Fe(N_2)_2$ (**5**) as precatalyst. Raw data shown as black points, overall simulation as a grey line, with components in green, blue and red (see Table for parameters). The spectrum was collected at 80 K with a parallel applied magnetic field of 50 mT.

Fitting details for Figure S59 Mössbauer spectrum collected after rapid-freeze-quenching a catalytic *reaction* after 30 minutes using (P2PPh)Fe(N2)$_2$ (5) as precatalyst. Raw data shown as black points, overall simulation as a grey line, with components in green, blue and red (see Table for parameters). The spectrum was collected at 80 K with a parallel applied magnetic field of 50 mT. Various fits were attempted for the Mössbauer spectrum. The species could be fit with one quadruple doublet with a large linewidth. A better fit was obtained by fitting the spectrum with two quadrupole doublets with slightly different parameters. Of the several options, one gave a species with a similar isomer shift (0.26 mm/s) and quadrupole splitting (1.12 mm/s) as observed in the reactions with **2**.

Component	δ (mm s^{-1})	ΔE_Q (mm s^{-1})	Linewidths, Γ (mm s^{-1})	Relative area
A	0.16	1.00	0.41	0.20
B	0.26	1.12	0.52	0.80

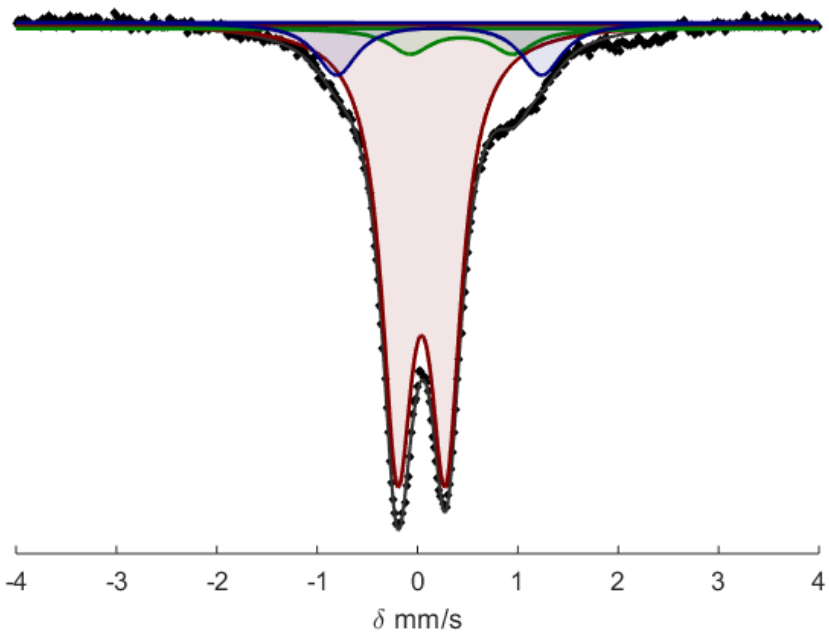

Figure S61 Mössbauer spectrum collected from a catalytic reaction warmed to room temperature using (P_2P^{Ph})Fe(N_2)$_2$ (**5**) as precatalyst. Raw data shown as black points, overall simulation as a grey line, with components in green, blue and red (see Table for parameters). The spectrum was collected at 80 K with a parallel applied magnetic field of 50 mT.

Fitting details for Figure S61: Three quadrupole doublet were found to be necessary to obtain an adequate simulation. The major species in the spectrum can be well simulated as (P_2P^{Ph})Fe(N_2)(H_2). The residual signal exhibits two quadrupole doublets and a broad feature. The broad feature, potentially due to a magnetically split species, could not be fit. The remaining quadrupole doublets could be fit as two species with respective areas of 0.05 and 0.13.

Component	δ (mm s^{-1})	ΔE_Q (mm s^{-1})	Linewidths, Γ (mm s^{-1})	Relative area
A	0.04	0.48	0.37	0.82
B	0.20	2.08	0.50	0.05
C	0.45	1.02	0.50	0.13

Crystallographic Details and Tables

[(P_2P^{Ph})Fe(N_2)$_2$(H)][BAr^F_4] (**7**) This structure contains disorder in the CF_3 moieties of the BAr^F_4 anion which could only be poorly modeled. B level alerts persist due to this disorder.

[(P_2P^{Ph})Fe(N_2)(H)][K(18-crown-6)] (**9**) This structure contains residual electron density assignable to disordered solvent molecules. OLEX2 was used to identify voids and a solvent mask was applied. This application gave a good improvement of data statistics. In addition, A level alerts persist [PLAT360, PLAT 410] in the checkcif file related to treated disorder about an 18-crown-6 molecule that is positioned on a mirror plane

CCDC 1824471-1824478 contains the supplementary crystallographic data for this paper. These data can be obtained free of charge from The Cambridge Crystallographic Data Centre via www.ccdc.cam.ac.uk/data_request/cif

Compound	**3**	**5**
Identification code	p17260	p17278
Empirical formula	$C_{30}H_{41}Br_{1.03}FeP_3$	$C_{30}H_{41}FeN_4P_3$
Formula weight	632.69	606.43
Temperature/K	99.97	99.99
Crystal system	triclinic	monoclinic
Space group	P-1	$P2_1/c$
a/Å	9.4966(10)	17.626(2)
b/Å	9.5930(8)	10.7764(8)
c/Å	17.630(3)	16.1774(19)
α/°	101.894(6)	90
β/°	96.481(6)	98.630(3)
γ/°	102.236(4)	90
Volume/Å3	1515.2(3)	3038.0(5)
Z	2	4
ρcalcg/cm3	1.387	1.326
μ/mm-1	2.032	0.681
F(000)	656	1280
Crystal size/mm3	0.187 × 0.163 × 0.02	0.16 × 0.15 × 0.076
Radiation	MoKα (λ = 0.71073)	MoKα (λ = 0.71073)
2Θ range for data collection/°	4.448 to 55.118	4.444 to 64.162
Index ranges	$-12 \le h \le 12$, $-12 \le k \le 12$, $-22 \le l \le 22$	$-26 \le h \le 26$, $-16 \le k \le 16$, $-24 \le l \le 24$
Reflections collected	87122	112007
Independent reflections	7004 [R_{int} = 0.0784, R_{sigma} = 0.0244]	10593 [R_{int} = 0.0944, R_{sigma} = 0.0420]
Data/restraints/parameters	7004/0/345	10593/3/381
Goodness-of-fit on F2	1.061	1.114
Final R indexes [I>=2σ (I)]	R_1 = 0.0232, wR_2 = 0.0557	R_1 = 0.0385, wR_2 = 0.1013
Final R indexes [all data]	R_1 = 0.0272, wR_2 = 0.0573	R_1 = 0.0583, wR_2 = 0.1167
Largest diff. peak/hole / e Å-3	0.53/-0.37	1.39/-0.95

Compound	**7**	**8**
Identification code	p17303	p17651
Empirical formula	$C_{129}H_{106}B_2F_{48}Fe_2N_8P_6$	$C_{42}H_{65}FeKN_2O_6P_3$
Formula weight	2999.35	877.47
Temperature/K	100	100
Crystal system	monoclinic	monoclinic
Space group	$P2_1/n$	$P2_1/n$
a/Å	22.4451(18)	10.4864(6)
b/Å	12.1053(6)	23.9154(17)
c/Å	25.482(2)	17.8619(10)
α/°	90	90
β/°	101.904(4)	93.645(3)
γ/°	90	90
Volume/Å3	6774.6(9)	4470.5(5)
Z	2	4
ρcalcg/cm3	1.47	1.304
μ/mm-1	3.434	0.584
F(000)	3040	1859
Crystal size/mm3	0.284 × 0.142 × 0.06	0.26 × 0.26 × 0.23
Radiation	CuKα (λ = 1.54178)	MoKα (λ = 0.71073)
2Θ range for data collection/°	5.886 to 159.312	4.248 to 79.494
Index ranges	$-28 \le h \le 28$, $-14 \le k \le 15$, $-32 \le l \le 31$	$-18 \le h \le 18$, $-42 \le k \le 42$, $-31 \le l \le 32$
Reflections collected	86754	220099
Independent reflections	14524 [R_{int} = 0.0840, R_{sigma} = 0.0509]	26751 [R_{int} = 0.0480, R_{sigma} = 0.0334]
Data/restraints/parameters	14524/800/907	26751/0/544
Goodness-of-fit on F2	1.022	1.061
Final R indexes [I>=2σ (I)]	R_1 = 0.0967, wR_2 = 0.2547	R_1 = 0.0460, wR_2 = 0.0998
Final R indexes [all data]	R_1 = 0.1178, wR_2 = 0.2737	R_1 = 0.0682, wR_2 = 0.1080
Largest diff. peak/hole / e Å-3	2.19/-0.84	2.07/-0.65

Compound	**9**	**10**
Identification code	p17634Pnma	p17581
Empirical formula	$C_{40}H_{61}FeKN_2O_4P_3$	$C_{42}H_{65}FeK_2N_2O_3P_3$
Formula weight	816.72	872.92
Temperature/K	100(2)	100
Crystal system	orthorhombic	monoclinic
Space group	Pnma	P21/n
a/Å	25.9569(13)	14.6713(13)
b/Å	17.0296(9)	16.6256(9)
c/Å	12.1851(6)	18.7129(12)
α/°	90	90
β/°	90	102.506(3)
γ/°	90	90
Volume/Å3	5386.2(5)	4456.1(5)
Z	4	4
ρcalcg/cm3	1.007	1.301
μ/mm-1	0.478	0.671
F(000)	1728	1856
Crystal size/mm3	0.22 × 0.16 × 0.12	0.22 × 0.199 × 0.055
Radiation	MoKα (λ = 0.71073)	MoKα (λ = 0.71073)
2Θ range for data collection/°	4.586 to 55.012	5.088 to 66.06
Index ranges	$-33 \le h \le 33, -20 \le k \le 22, -15 \le l \le 15$	$-22 \le h \le 22, -24 \le k \le 25, -28 \le l \le 25$
Reflections collected	73356	64947
Independent reflections	6368 [R_{int} = 0.0545, R_{sigma} = 0.0235]	15164 [Rint = 0.0574, Rsigma = 0.0787]
Data/restraints/parameters	6368/303/287	15164/0/486
Goodness-of-fit on F2	1.123	1.014
Final R indexes [I>=2σ (I)]	R_1 = 0.1026, wR_2 = 0.3059	R1 = 0.0569, wR2 = 0.1094
Final R indexes [all data]	R_1 = 0.1162, wR_2 = 0.3201	R1 = 0.1074, wR2 = 0.1263
Largest diff. peak/hole / e Å-3	3.98/-1.50	1.56/-0.61

Compound	**11**
Identification code	p17555
Empirical formula	$C_{33}H_{50}FeKN_2P_3Si$
Formula weight	690.7
Temperature/K	124.99
Crystal system	orthorhombic
Space group	$P2_12_12_1$
a/Å	10.5863(9)
b/Å	16.3326(12)
c/Å	20.8095(17)
α/°	90
β/°	90
γ/°	90
Volume/Å3	3598.0(5)
Z	4
ρcalcg/cm3	1.275
μ/mm-1	6.154
F(000)	1464
Crystal size/mm3	0.164 × 0.077 × 0.059
Radiation	CuKα (λ = 1.54178)
2Θ range for data collection/°	6.88 to 158.208
Index ranges	$-12 \leq h \leq 13$, $-19 \leq k \leq 20$, $-26 \leq l \leq 24$
Reflections collected	38615
Independent reflections	7481 [R_{int} = 0.0728, R_{sigma} = 0.0653]
Data/restraints/parameters	7481/0/382
Goodness-of-fit on F2	1.062
Final R indexes [I>=2σ (I)]	R_1 = 0.0670, wR_2 = 0.1490
Final R indexes [all data]	R_1 = 0.0873, wR_2 = 0.1606
Largest diff. peak/hole / e Å-3	1.31/-0.81

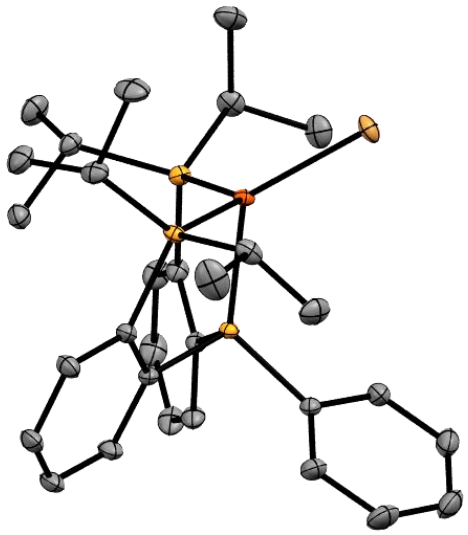

Figure S62 ORTEP depiction of the solid-state molecular structure of **4** (displacement ellipsoids are shown at the 50% probability; hydrogens atoms and disorder from cocrystalized **3** are omitted for clarity).

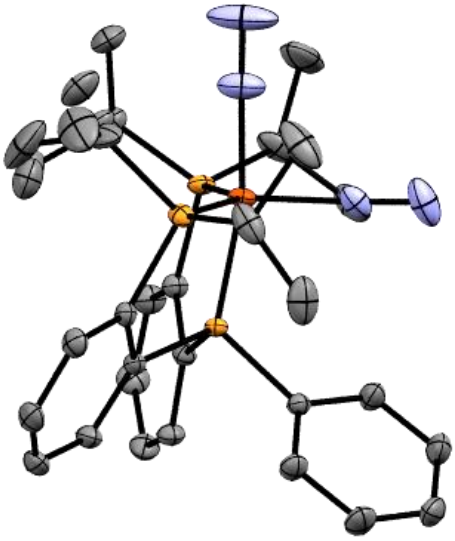

Figure S63 ORTEP depiction of the solid-state molecular structure of **5** (displacement ellipsoids are shown at the 50% probability; hydrogens atoms are omitted for clarity).

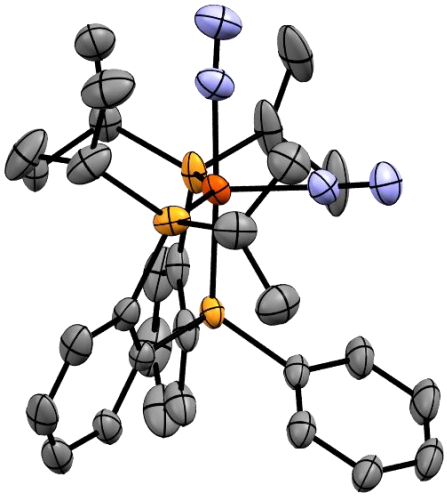

Figure S64 ORTEP depiction of the solid-state molecular structure of **7** (displacement ellipsoids are shown at the 50% probability; hydrogens atoms, BAr^{F}_{4} and disordered solvent molecules are omitted for clarity).

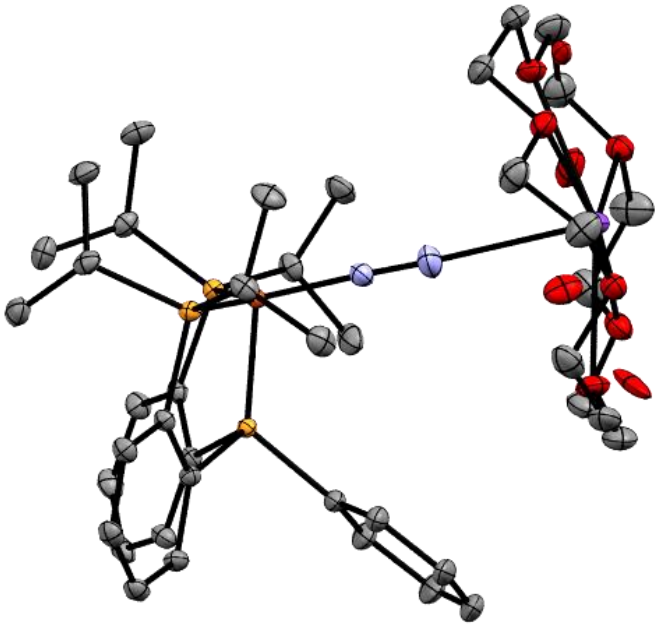

Figure S65 ORTEP depiction of the solid-state molecular structure of **8** (displacement ellipsoids are shown at the 50% probability; hydrogens atoms are omitted for clarity).

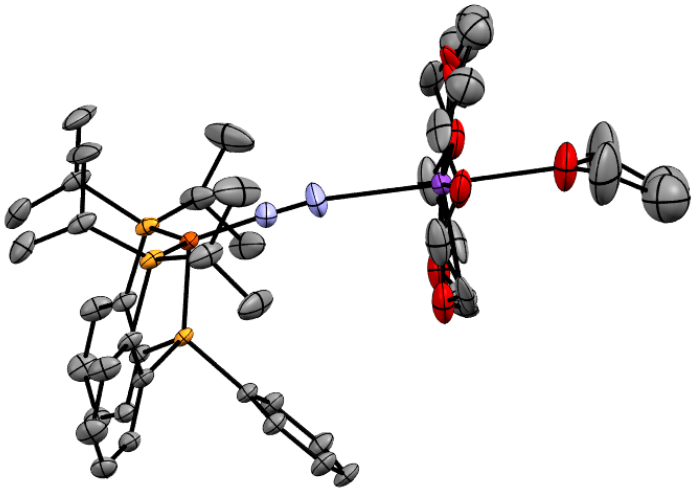

Figure S66 ORTEP depiction of the solid-state molecular structure of **9** (displacement ellipsoids are shown at the 50% probability; hydrogens atoms are omitted for clarity).

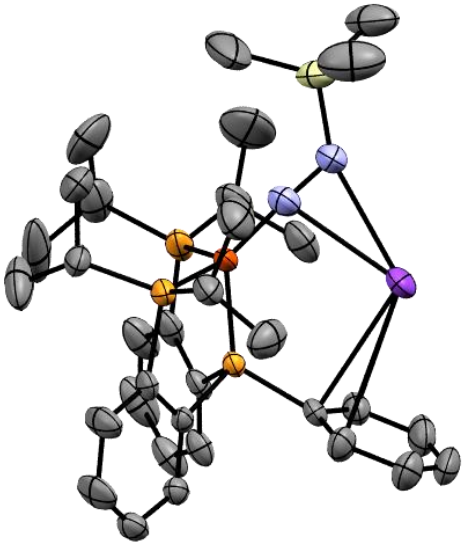

Figure S67 ORTEP depiction of the solid-state molecular structure of **11** (displacement ellipsoids are shown at the 50% probability; hydrogens atoms are omitted for clarity).

DFT Calculations

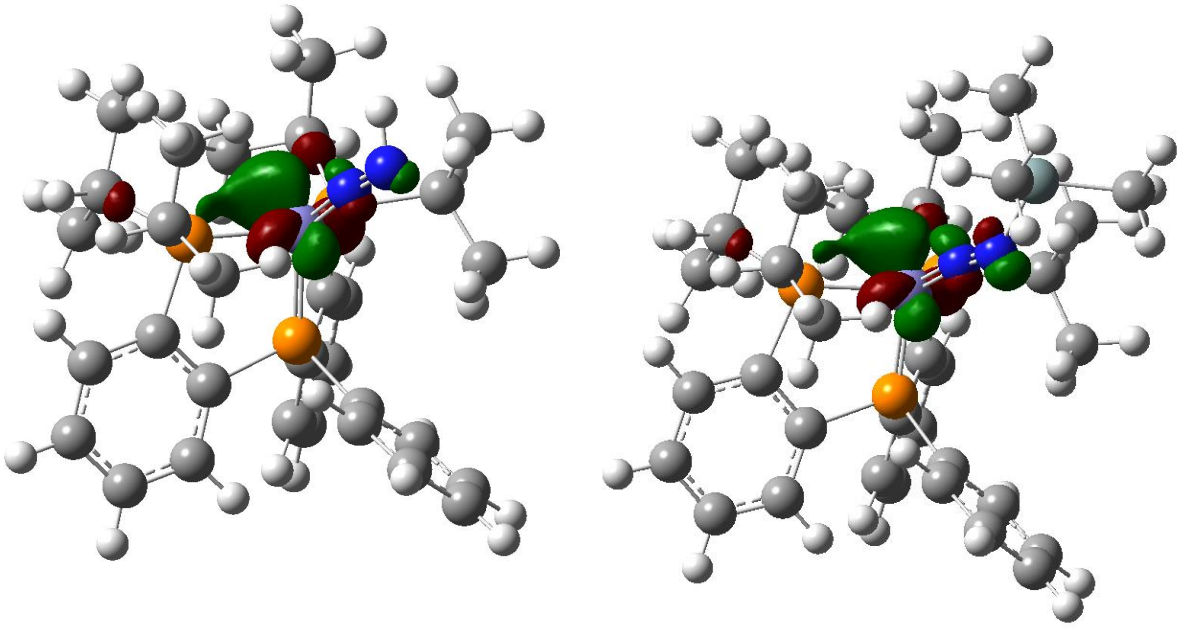

Figure S68 Density function theory calculated molecular orbitals. (Left) HOMO of $[(P_2P^{Ph})Fe(NNH)]^-$ and (Right) HOMO of $[(P_2P^{Ph})Fe(NNTMS)]^-$ (isovalue = 0.06).

Table S8 A comparison of gas phase optimized and experimental bond parameters demonstrating the good agreement between optimized gas-phase structures of $[(P_2P^{Ph})Fe(NNTMS)]^-$, $[(P_2P^{Ph})Fe(NNH)]^-$ and experimental values from X-ray data of $[(P_2P^{Ph})Fe(NNTMS)]K$.

Species	**Fe-N (Å)**	**Fe-P^{Ph} (Å)**	**N-N (Å)**
$[(P_2P^{Ph})Fe(NNTMS)]K$ (XRD)	1.664(7)	2.115(2)	1.270(9)
$[(P_2P^{Ph})Fe(NNTMS)]^-$	1.662	2.112	1.244
$[(P_2P^{Ph})Fe(NNH)]^-$	1.669	2.111	1.250

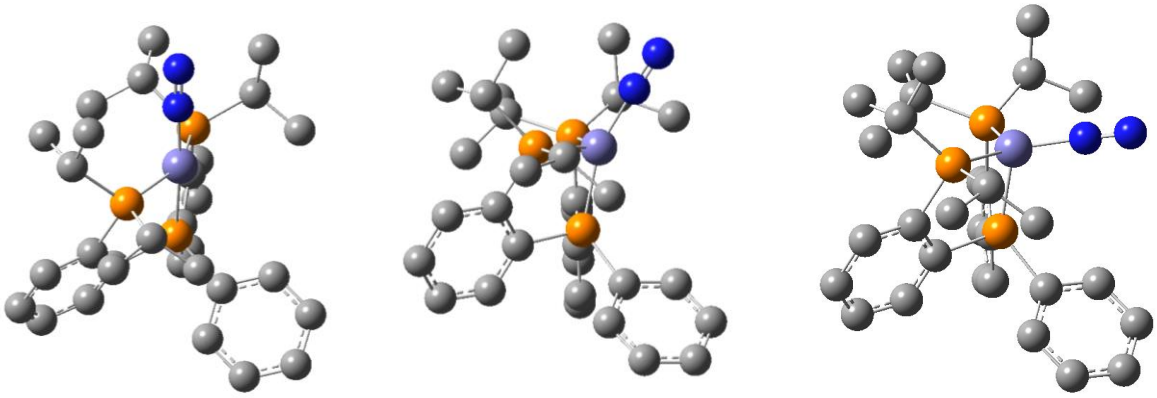

Figure S69 The gas-phase optimized geometry of $(P_2P^{Ph})Fe(N_2)$ with different spin states and geometries. (Left) S = 0, (Middle) S = 1 and (Right) S = 1.

Table S9 Energies of gas-phased optimized geometries of $(P_2P^{Ph})Fe(N_2)$. The energies are given relative to the lowest energy triplet state

Species	Spin State	Energy (kcal mol^{-1})	N–N (Å)	P^{Ph}–Fe–N (°)	νN_2 (cm^{-1})
$(P_2P^{Ph})Fe(N_2)$	S = 0	7.4	1.145	173.8	2076.7
$(P_2P^{Ph})Fe(N_2)$	S = 1	1.3	1.141	159.1	2093.4
$(P_2P^{Ph})Fe(N_2)$	S = 1	0	1.142	106.5	2093.2

Supplementary References

(1) Buscagan, T. M.; Oyala, P. H.; Peters, J. C. N_2-to-NH_3 Conversion by a triphos–iron catalyst and enhanced turnover under photolysis. *Angew. Chem. Int. Ed.* **2017**, *56*, 6921–6926.

(2) Del Castillo, T. J.; Thompson, N. B.; Peters, J. C. A synthetic single-site Fe nitrogenase: high turnover, freeze-quench ^{57}Fe Mössbauer data, and a hydride resting state. *J. Am. Chem. Soc.* **2016**, *138*, 5341–5350.

(3) Robbins, J. L.; Edelstein, N.; Spencer, B.; Smart, J. C. Syntheses and Electronic Structures of Decamethylmetallocenes. *J. Am. Chem. Soc.* **1982**, *104* (7), 1882–1893.

(4) Weitz, I. S.; Rabinovitz, M. The application of C_8K for organic synthesis: reduction of substituted naphthalenes. *J. Chem. Soc. Perkin Trans.* **1993**, *1*, 117.

(5) Evans, D. F. The determination of the pararnagnetic susceptibility of substances in solution by nuclear magnetic resonance. *J. Chem. Soc.* **1959**, 2003–2005.

(6) Gaussian 09, Revision A.02, Frisch, M. J.; Trucks, G. W.; Schlegel, H. B.; Scuseria, G. E.; Robb, M. A.; Cheeseman, J. R.; Scalmani, G.; Barone, V.; Petersson, G. A.; Nakatsuji, H.; Li, X.; Caricato, M.; Marenich, A.; Bloino, J.; Janesko, B. G.; Gomperts, R. ; Mennucci, B.; Hratchian, H. P.; Ortiz, J. V.; Izmaylov, A. F.; Sonnenberg, J. L.; Williams-Young, D.; Ding, F.; Lipparini, F.; Egidi, F.; Goings, J.; Peng, B.; Petrone, A.; Henderson, T.; Ranasinghe, D.; Zakrzewski, V. G.; Gao, J.; Rega, N.; Zheng, G.; Liang, W.; Hada, M.; Ehara, M.; Toyota, K.; Fukuda, R.; Hasegawa, J.; Ishida, M.; Nakajima, T.; Honda, Y.; Kitao, O.; Nakai, H.; Vreven, T.; Throssell, K.; Montgomery, Jr., J. A.; Peralta, J. E.; Ogliaro, F.; Bearpark, M.; Heyd, J. J.; Brothers, E.; Kudin, K. N.; Staroverov, V. N.; Keith, T.; Kobayashi, R.; Normand, J.; Raghavachari, K.; Rendell, A.; Burant, J. C.; Iyengar, S. S.; Tomasi, J.; Cossi, M.; Millam, J. M.; Klene, M. ; Adamo, C.; Cammi, R.; Ochterski, J. W.; Martin, R. L.; Morokuma, K.; Farkas, O.; Foresman, J. B.; Fox, D. J. Gaussian, Inc., Wallingford CT, 2016

(7) Tao, J.; Perdew, J. P.; Staroverov, V. N.; Scuseria, G. E. Climbing the Density Functional Ladder: Nonempirical Meta–generalized Gradient Approximation Designed for Molecules and Solids. *Phys. Rev. Lett.* **2003**, *91* (14), 3–6.

(8) Weigend, F.; Ahlrichs, R. Balanced basis sets of split valence, triple zeta valence and quadruple zeta valence quality for H to Rn: design and assessment of accuracy. *Phys. Chem. Chem. Phys.* **2005**, *7*, 3297–3305.

(9) Pfirrmann, S.; Limberg, C.; Herwig, C.; Knispel, C.; Braun, B.; Bill, E.; Stösser, R. A reduced β-diketiminato-ligated Ni_3H_4 unit catalyzing H/D Exchange. *J. Am. Chem. Soc.* **2010**, *132*, 13684–13691.

(10) Creutz, S. E.; Peters, J. C. Spin-state tuning at pseudo-tetrahedral d^6 ions: spin crossover in $[BP_3]Fe^{II}$–X complexes. *Inorg. Chem.* **2016**, *55*, 3894–3906.

(11) Rittle, J.; Mccrory, C. C. L.; Peters, J. C. A 10^6 fold enhancement in N_2 binding affinity of an $Fe_2(\mu\text{-}H)_2$ core upon reduction to a mixed-valence $Fe^{II}Fe^{I}$ state. *J. Am. Chem. Soc.* **2014**, *136*, 13853–13862.

(12) Tepper, A. W. J. W.; Bubacco, L.; Canters, G. W. Paramagnetic properties of the halide-bound derivatives of oxidised tyrosinase investigated by ^{1}H NMR spectroscopy. *Chem. - A Eur. J.* **2006**, *12*, 7668–7675.

(13) Zaballa, M. E.; Ziegler, L.; Kosman, D. J.; Vila, A. J. NMR study of the exchange coupling in the trinuclear cluster of the multicopperoxidase Fet3p. *J. Am. Chem. Soc.* **2010**, *132*, 11191–11196.